Sesorless startup of a PMSM for a hybrid electric vehicle application

by

Alejandro Martínez Alonso

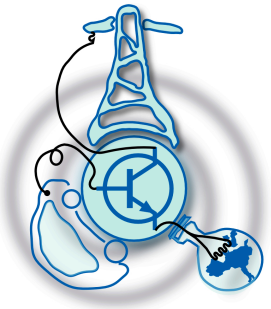

Submitted to the Department of Electrical Engineering, Electronics, Computers and Systems
in partial fulfillment of the requirements for the degree of
Electrical Energy Conversion and Power Systems (EECPS) Master
at the
UNIVERSIDAD DE OVIEDO
July 2016

Author .....

Certified by .....
David Díaz Reigosa
Associate Professor
Thesis Supervisor

Certified by .....
Cristian Blanco Charro
Dr.
Thesis Supervisor

Sesorless startup of a PMSM for a hybrid electric vehicle application

by

Alejandro Martínez Alonso

Submitted to the Department of Electrical Engineering, Electronics, Computers and Systems
on July 15, 2016, in partial fulfillment of the
requirements for the degree of
Electrical Energy Conversion and Power Systems (EECPS) Master

Abstract

In this master thesis, a sensorless control strategy of a permanent magnet synchronous machine for its application to a hybrid electric vehicle is implemented. An analysis about the benefits of implementing this kind of control strategy and a study of the most important sensorless control methods that are used nowadays along with the implementation of the different control loops that this kind of control strategy implies will be done in order to perform different simulations in SIMULINK tool of MATLAB that prove the correct operation of the electric machine under this kind of control. Moreover, some tests will be carried out with the real electric machine to check its real behaviour when it operates under this control strategy.

Keywords

Permanent magnet synchronous machine, sensorless, Electric vehicle, filter, High frequency, Back ElectroMotiveForce, Induction machine, Phase Locked Loop

Thesis Supervisor: David Díaz Reigosa
Title: Associate Professor

Thesis Supervisor: Cristian Blanco Charro
Title: Dr.

Acknowledgments

Lo primero de todo querría dar las gracias a mi director de tesis, Profesor Titular David Díaz Reigosa. Gracias por su cercanía y disponibilidad, asi como a su gran conocimiento que ha hecho posible la realizacion de esta tesis fin de master.

Ademas, querría agradecer su gran esfuerzo a mi co-tutor de tesis, Dr. Cristian Blanco Charro. Gracias por tu infinita paciencia y la gran ayuda prestada dia tras dia, ya que sin ella hubiera sido mucho mas dificil realizar este proyecto.

Quería también aprovechar esta sección para expresar mi gratitud a Daniel Fernandez, ya que sus brillantes ideas y el gran conocimiento prestado me ha ayudado de una manera increible al desarrollo de la presente tesis.

También querría dar las gracias a Cristina, mi gran apoyo en todo momento, ya que sin ella hubiera sido imposible acabar este proyecto, te lo debo todo. Aprovecho también para dar las gracias a la familia de Cristina, mi segunda familia, en donde se incluye Flecha, un gran apoyo que no se aprecia a simple vista.

Por ultimo, querría dar las gracias a mi familia. A mis padres, Manuel y Raquel, mi verdadero apoyo durante todo este tiempo y que han tenido que estar ahí días tras día apoyandome en todo, muchisimas gracias. Y gracias también a mis tíos, abuelos y primos, que me han ayudado en todo lo posible y han hecho más fácil que llegue hasta donde estoy actualmente. Gracias a todos.

Contents

List of Figures

List of Tables

Glosary

Acronyms

ATO	Angle Tracking Observer
BEMF	Back ElectroMotiveForce
BPF	Band-Pass Filter
BSF	Band-Stop Filter
EV	Electric Vehicle
HEV	Hybrid Electric Vehicle
HF	High frequency
HPF	High-Pass Filter
IM	Induction Machine
IPMSM	Interior Permanent Magnet Synchronous Machine
LPF	Low-Pass Filter
PI controller	Proportional-Integral controller
PLL	Phase Locked Loop
PMSM	Permanent Magnet Synchronous Machine
SPMSM	Surface Permanent Magnet Synchronous Machine
SRF PLL	Synchronous Reference Frame PLL

Chapter 1

Introduction

1.1 Thesis motivation

In the last decades, Permanent Magnet Synchronous Machines (PMSMs) have experienced a very important growth in their use in industry applications. This is due to the more and more strict performances that are required for the machines in this scope.

For the actual industry applications, PMSMs present better performances than other kind of electric machines, such as induction machines (IMs), which are the most common in the industry. One of the most important characteristics that they have is their very high efficiency, no excitation current is needed in the rotor since these kind of machines are excited by means of the magnets, so that the only losses that exists are the iron losses which mostly occur in the stator. Moreover, another important characteristic is the high power density that they have, which is a very demanded characteristic, since in a small area these machines can deliver a high amount of power. In general, PMSMs are smaller and have a higher efficiency than other kind of electric machines of the same power, so that in addition to present better characteristics they can be easier installed. All of these characteristics make PMSMs suitable for industry applications, being the most demanded markets in which they are used the power generation industry, medical technology, aerospace industry, compressors and pumps or vehicle applications, being this last one a very demanded

market nowadays.

The most important drawback of this kind of machines is their high cost, the magnets that they use are very expensive and represents a high percentage of the total cost of the machine. Due to this, the cost reduction of the part that has to do with the design and cabling becomes in a very important part of the machine development for maintaining the total cost inside acceptable limits. This field is in which this master thesis is focused on.

PMSM control is achieved by knowing the position of the magnets at any moment, so that a position sensor is usually placed in the rotor of the machine in order to obtain it. However this sensor it is very expensive, so that a control strategy of the machine without this sensor and the associated cabling it is the challenge that many companies face nowadays. With this new situation, where there is no position sensor in the rotor of the machine, different control techniques must be used in order to obtain the position of the rotor at any moment in order to properly control the PMSM and this is what is called **sensorless control strategy**.

This kind of control strategy is being very demanded for different industry applications due to its important benefits, since along with the high cost reduction that it implies due to the elimination of the position sensor and its cabling, a more compact machine and easy to install is achieved. However, the problem related to this control has to do with the higher complexity that it implies.

For this project, the most extended sensorless control techniques that are currently used will be implemented and tested, which are the **high frequency (HF) method** that consists in a high frequency signal injection that allows to obtain the rotor position of the electric machine at low or zero speed, and the **back electromotive force (BEMF) method** which allows to obtain the machine rotor position at medium or high speed ranges. This last one method is based on the back electromotive force generated by the machine, so that this method will not operate at zero or low speeds since the generated BEMF will be zero.

Then, inside PMSMs, several groups can be distinguished depending on the position of the magnets along the rotor. Depending on this, PMSMs can be classified

into Surface PMSMs (SPMSMs) or Interior PMSMs (IPMSMs). Then, inside these two groups, several configurations can be adopted, being SPMSMs divided into Surface mounted magnets PMSMs (**SM-PMSMs**) and Inset surface magnets PMSM (**SI-PMSMs**), and IPMSMs divided into classical internal (buried) magnets PMSMs (**I-PMSM**), V-shaped internal magnets PMSMs (**VI-PMSMs**) and rotor with radial internal magnets PMSMs (**RI-PMSMs**). Fig.1-1 shows all of these PMSMs configurations [1].

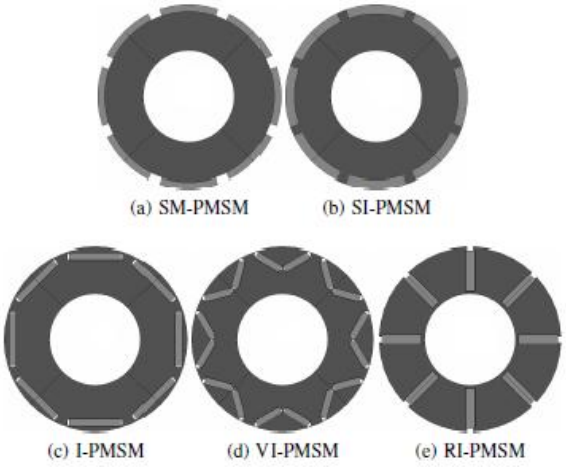

Figure 1-1: PMSMs configurations.

Looking at Fig.1-1, the PMSM that is going to be used along this master thesis for simulations and real tests under sensorless control strategy is a **SM-PMSM** with outer rotor configuration, which will be introduced in **section 3.1.1**.

1.2 Objectives

After being introduced the master thesis topic, the objectives that are expected to be achieved are the following ones:

1. Understanding the important advantages, the benefit, of using a sensorless control strategy against using the classical control based on the use of sensors in the rotor of the machine.

2. Theoretical study of the most extended sensorless control techniques applied to PMSMs, understanding their basic principles and how they work.

3. Implementation of an algorithm that allows the transition between different sensorless methods in a smooth way depending on the machine speed.

4. Implementation and simulation of the complete system that conforms the PMSM operating under sensorless control strategy at different speeds in order to analyse the combined operation of the sensorless methods.

5. Real tests of the PMSM that allows to analyse the real behaviour of the electric machine under this kind of control strategy.

1.3 Structure of the thesis

The present master thesis is divided into six chapters, being each one of them focused on the following information:

- **Chapter 1:** In this chapter, an introduction about the master thesis topic has been done along with an individual description of each one of the proposed objectives.

- **Chapter 2:** Along this chapter, a review of the most extended sensorless control methods applied to PMSMs that are used nowadays is done, explaining in which situation they are used depending on the machine speed. An introduction for each method is performed and the PMSM equations in which are based each one of them are presented. Moreover, the control loops of both sensorless control methods are explained in detail and some important selection criteria that have to do with these methods, such as the HF signal selection that is injected, are also presented.

- **Chapter 3:** Along this chapter, the sensorless control methods implementation that is done for being able to simulate the machine operation under this kind

of control strategy is explained in detail, including filters design, tuning of the different PI controllers and different important criteria that have to be taken into account for the correct operation of the electric machine. A description about the PMSM that is used in the present thesis for simulation and real analysis, and about the control scheme that governs the operation of this electric machine it is also done.

- **Chapter 4:** In this chapter, the obtained simulation results of the PMSM operation under sensorless control strategy are presented. The simulation is performed in SIMULINK tool of MATLAB. At first, both sensorless methods are independently analysed in order to check if they are working properly, and then, the complete system is analysed, which consists on the PMSM operating under both sensorless methods with a determined speed profile that allows to check the performance of the machine at any possible situation.

- **Chapter 5:** Along this chapter, the experimental results that were obtained from some tests with the real PMSM operating under the developed sensorless control are presented. The most important signals that corroborate the PMSM properly operation are analysed.

- **Chapter 6:** In this last chapter, the extracted conclusions of this master thesis and the future work that can be done in this field are presented.

Chapter 2

Sensorless control methods

2.1 Introduction

Sensorless control techniques are broadly used nowadays in many different applications. This is due to the important advantages that this kind of control implies, being the most important the following ones [2]:

- **Cost:** As there are no sensors included in the rotor of the PMSM the total cost of the project is reduced. Adding sensors to the rotor leads to a higher system complexity since flexible PCBs or slip rings, among others, should be included in the machine in order to obtain the rotor position which suppose a very high cost increment for the final project.

- **Reliability:** Not including sensors in the PMSM rotor increases the reliability of the system because any possible failure in the measurements that these kind of sensors provide could make the control loops of the systems to fail, implying the machine failure, so sensorless control techniques make the system more robust, which is very important in the case of military applications. Moreover, with this situation no maintenance related to the sensors should be done, so the cost is also reduced.

- **Noise immunity:** As sensors are not included in the rotor of the PMSM, the noise that could be induced by them due to the machine operation is avoided,

which is so useful for the machine performance allowing control loops working in a properly way without any extra circuits in order to avoid this noise.

However, the implementation of this kind of control strategy implies using different PMSM control methods that allow to obtain the rotor position of the electric machine. These methods are divided into three groups, the first one based on fundamental excitation methods, the second one based on saliency and signal injection methods and the third one based on artificial intelligence methods [2],[3].

Fundamental excitation methods

Inside this group of sensorless control methods, we can distinguish the non-adaptive and the adaptive methods.

As for the non-adaptive sensorless control methods they use current and voltage measurements of the machine as well as the machine equations. The benefits of using this kind of control methods are the very quick response that they have and the easy to be computed, but very accurate PMSM parameters are required. **Estimators using stator voltage or currents, flux based position estimators or estimators based on the BEMF** are examples of this kind of sensorless control methods.

Respect to the adaptive methods they use the mathematical model of the machine and input variables measurements providing estimated outputs. Then, the error is fed back to the system model to correct the estimated values in order to adapt them. The most important advantage of these methods is the possibility of estimate all the possible states of the machine, but they require a very complicated algorithm and a high computational cost.

Saliency and signal injection methods

This kind of sensorless control methods use the salient-pole PMSMs characteristic where the inductance varies with the rotor position, so that a HF (high frequency) signal (voltage or current) is injected and by signal processing it is possible to extract the current components that contain the rotor position information of the electric machine.

Artificial intelligence methods

The artificial intelligence methods are proposed as a way to identify and control non-linear dynamic systems because of the wide range of non-linear functions of any desired degree and accuracy that they can approximate. These methods have the advantages of immunity against harmonic ripples and robustness to parameters variations. However, these methods have a very high complexity as they include neural networks, real time algorithm calculations and a high computational cost.

Among all of these sensorless control methods, the **BEMF** and the **HF** methods, which are the most extended ones [2],[3],[4], are going to be explained in detail along this master thesis.

2.1.1 PMSM dynamic model

The dynamic model of the PMSM it is presented below. The stator voltage model in the rotor reference frame is given by [5],[6]:

$$\begin{bmatrix} V_{ds}^r \\ V_{qs}^r \end{bmatrix} = \begin{bmatrix} R_s & 0 \\ 0 & R_s \end{bmatrix} \begin{bmatrix} i_{ds}^r \\ i_{qs}^r \end{bmatrix} + \begin{bmatrix} p & -w_r \\ w_r & p \end{bmatrix} \begin{bmatrix} \lambda_{ds}^r \\ \lambda_{qs}^r \end{bmatrix} \tag{2.1}$$

Where **p** term represents the derivative term and λ_{dq} represents the fluxes in both axes. Then, these fluxes are expressed as:

$$\begin{bmatrix} \lambda_{ds}^r \\ \lambda_{qs}^r \end{bmatrix} = \begin{bmatrix} L_{ds} & 0 \\ 0 & L_{qs} \end{bmatrix} \begin{bmatrix} i_{ds}^r \\ i_{qs}^r \end{bmatrix} + \begin{bmatrix} \lambda_{pm} \\ 0 \end{bmatrix} \tag{2.2}$$

Being λ_{pm} the permanent magnet flux. Substituting equation 2.2 into equation 2.1, the voltages in both axes can be obtained.

$$V_{ds}^r = R_s i_{ds}^r + pL_{ds} i_{ds}^r - w_r L_{qs} i_{qs}^r \tag{2.3}$$

$$V_{qs}^r = R_s i_{qs}^r + pL_{qs} i_{qs}^r + w_r L_{ds} i_{ds}^r + w_r \lambda pm \tag{2.4}$$

Being $w_r \lambda_{pm}$ the BEMF component.

These equations can be also transformed to the stator reference frame resulting

in the following stator voltage model [6],[7]:

$$\begin{bmatrix} V_{ds}^s \\ V_{qs}^s \end{bmatrix} = \begin{bmatrix} R_s + p(\Sigma L_s - \Delta L_s cos(2\theta_r)) & -p\Delta L_s sin(2\theta_r) \\ p\Delta L_s sin(2\theta_r) & R_s + p(\Sigma L_s + \Delta L_s cos(2\theta_r)) \end{bmatrix} \begin{bmatrix} i_{ds}^s \\ i_{qs}^s \end{bmatrix} + w_r \lambda_{pm} \begin{bmatrix} -sin(\theta_r) \\ cos(\theta_r) \end{bmatrix} \tag{2.5}$$

Where:

$\Delta L_s = \frac{L_{ds} - L_{qs}}{2}$ represents the differential inductance

$\Sigma L_s = \frac{L_{ds} + L_{qs}}{2}$ represents the average inductance

2.2 BEMF method

The BEMF control strategy is used to estimate the position and speed of the machine only when it is operating in medium or high speed ranges. This is because the BEMF is proportional to the speed of the machine (equation 2.4), so that at low speed ranges or zero speed of the machine, the information given by the BEMF vanishes and it is not useful, so it can not be used in these situations [6],[8].

This method is based on the PMSM equations in the stationary reference frame (α,β), which are developed in section 2.2.1 [9].

2.2.1 PMSM model in stationary reference frame

The BEMF control method is based on the PMSM equations in the stationary reference (α,β). This allows not to do reference frame transformations (i.e $\alpha\beta$ to dq) and the corresponding angle estimation, so that the control loop implementation becomes not so complex.

Equation 2.6 shows the PMSM model in the stationary reference frame (α,β) [9],[10]:

$$\begin{aligned} V_\alpha &= Ri_\alpha + e_\alpha + \frac{di_\alpha}{dt} L_q \\ V_\beta &= Ri_\beta + e_\beta + \frac{di_\beta}{dt} L_q \end{aligned} \tag{2.6}$$

Where $V_{\alpha,\beta}$ correspond to the PMSM terminal voltages, R is the PMSM winding resistance, $i_{\alpha,\beta}$ are the PMSM phase currents and $e_{\alpha,\beta}$ are the BEMF components.

The BEMF component can be presented as follows [10]:

$$\begin{aligned} e_\alpha &= \frac{d\Psi_\alpha}{dt} \\ e_\beta &= \frac{d\Psi_\beta}{dt} \end{aligned} \tag{2.7}$$

Where $\Psi_{\alpha,\beta}$ correspond to the PMSM flux linkage.

Substituting equation 2.7 into equation 2.6, the rotor flux linkage of the PMSM can be extracted as a function of the terminal voltages, phase currents and winding resistance of the PMSM. Equation 2.8 shows this procedure.

$$\begin{aligned} V_\alpha = Ri_\alpha + \frac{d\Psi_\alpha}{dt} + \frac{di_\alpha}{dt}L_q \Rightarrow \frac{d\Psi_\alpha}{dt} = V_\alpha - Ri_\alpha - \frac{di_\alpha}{dt}L_q \Rightarrow \boxed{\Psi_\alpha = \int (V_\alpha - Ri_\alpha)dt - i_\alpha L_q} \\ V_\beta = Ri_\beta + \frac{d\Psi_\beta}{dt} + \frac{di_\beta}{dt}L_q \Rightarrow \frac{d\Psi_\beta}{dt} = V_\beta - Ri_\beta - \frac{di_\beta}{dt}L_q \Rightarrow \boxed{\Psi_\beta = \int (V_\beta - Ri_\beta)dt - i_\beta L_q} \end{aligned} \tag{2.8}$$

2.2.2 BEMF control loop

For obtaining the speed and rotor position of the machine at medium or high speed ranges, the BEMF control loop shown in Fig.2-1 must be implemented, which is based on the equations explained in section 2.2.1.

Looking at Fig.2-1, going from the left to the right, the first step that is done is the transformation of the terminal voltages (V_a, V_b, V_c) and phase currents (i_a, i_b, i_c) of the machine from the abc reference frame to the $\alpha\beta$ reference frame. Then, equation 2.8 is implemented to obtain the rotor flux linkage $(\Psi_\alpha, \Psi_\beta)$ of the PMSM.

After that, a Phase Locked Loop (PLL) is implemented in order to obtain the speed and angle of the machine from the flux linkage.

Section 2.2.2.1 shows a study of different kinds of PLLs.

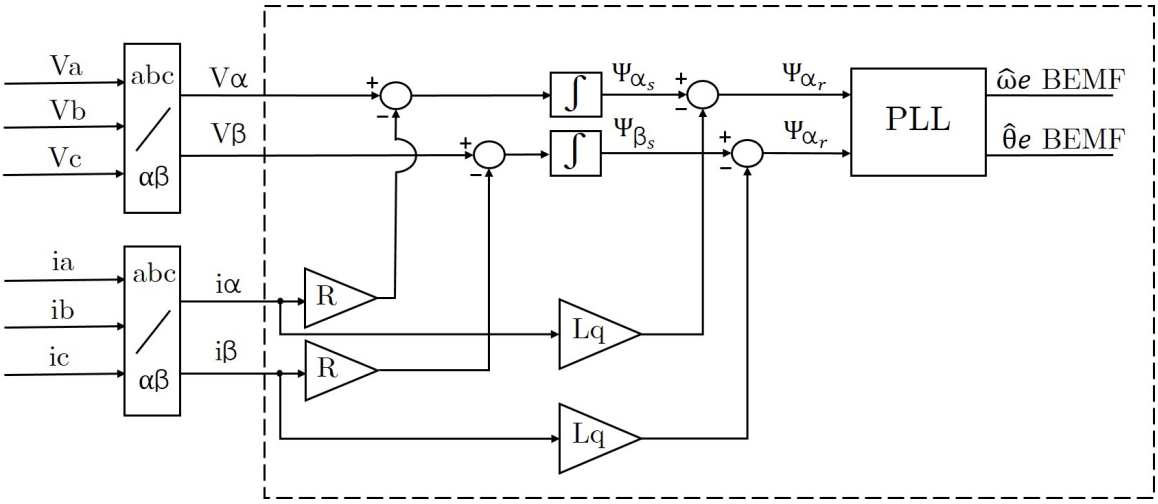

Figure 2-1: BEMF control loop.

2.2.2.1 Phase locked loop (PLL)

PLL techniques are broadly used nowadays in order to obtain the speed and position of electric machines because of their good characteristics, such as simplicity, good dynamic response and robustness.

There are mainly two basic PLL structures adequate for this purpose which are the **Synchronous Reference Frame PLL** (SRF PLL) and the **Angle Tracking Observer** (ATO) [11].

SRF PLL

The working principle of the SRF PLL consists of controlling the q-axis component to be zero, so that the d-axis component will be equal to the magnitude of the input signal. Fig.2-2 shows the block diagram of this PLL.

Looking at Fig.2-2, the input signal corresponds to the PMSM flux linkage in $\alpha\beta$ reference frame, as Fig.2-1 indicates. Then, starting from this signal a reference frame transformation to the dq reference frame is done and the corresponding Ψ_d and Ψ_q signals are obtained, being the first one equal to the PMSM flux linkage magnitude and the second one controlled to be zero.

After that, a PI controller allows to obtain the estimated PMSM speed, and by integrating it, the estimated PMSM rotor position can be obtained. Making the input

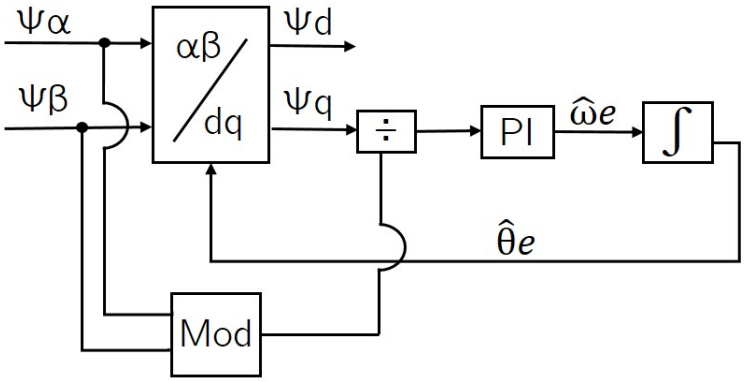

Figure 2-2: SRF PLL block diagram.

value of the PI controller unitary is always a good practise in order to make the error independent of the input signal magnitude [11]. For doing that, the q-axis value is divided by the module of the input signal in the $\alpha\beta$ reference frame at the input of the PI controller as it can be seen in Fig.2-2.

This PLL technique provides a very good performance, however, when the PLL input is unbalanced or contains harmonics components the estimated speed and position becomes inaccurate. In order to solve this problem, pre-filter stages or filters in the loop stages can be used to eliminate the different disturbances that can affect to the PLL before they reach it or the reduction of the PI controller bandwidth can be also applied, being this last one not so good for the dynamic response of the PLL [11].

The SRF PLL is the one that has been selected for the BEMF method that will be implemented in this project because of its relatively easier implementation compared with the ATO implementation, which is explained below.

ATO

The ATO, also known as $\alpha\beta$ PLL, is another kind of PLL that can be used in order to estimate the PMSM rotor position and speed. Fig.2-3 shows the block diagram of this PLL technique.

Attending to Fig.2-3, the input signal, which is abc reference frame, is transformed to the $\alpha\beta$, and then, the principle of operation of this kind of PLL is practically the

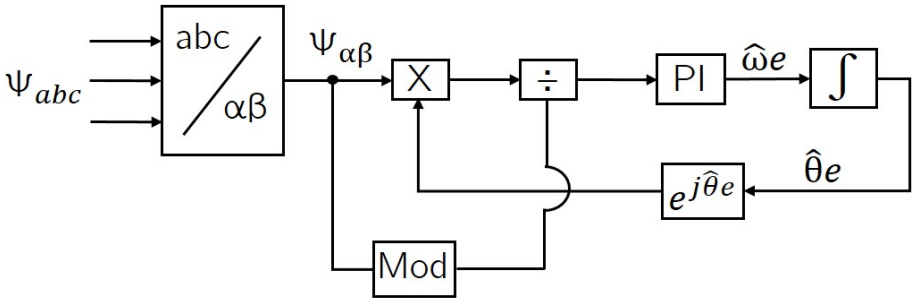

Figure 2-3: ATO block diagram.

same as the SRF PLL, a PI controller is used in order to obtain the estimated PMSM speed and by integrating it, the estimated rotor position can be obtained.

The main difference of using this method is that the phase error is obtained by the vectorial cross product between the input signal in the $\alpha\beta$ reference frame ($\Psi_{\alpha\beta}$) and the the estimated unitary vector $e^{j\hat{\theta}_e}$ [11]. In this case, the input of the PI controller is normalized by the same method as before.

As in the case of the SRF PLL, the ATO has the same problems with unbalances and harmonics contents in the PLL input, so that filtering stages or PI controller bandwidth reduction can be applied [11].

2.3 HF method

At zero and low speed ranges of the machine, the information given by fundamental excitation methods, such as the BEMF method, is not useful, being zero or not so accurate as it is proportional to the machine speed. For these situations, the high frequency signal injection method is the most common strategy that is used in order to obtain the speed and rotor position of the PMSM.

The HF signal injection method is based on the electric machine magnetic saliency phenomenon. In this method, a high frequency current or voltage signal is superimposed to the fundamental excitation of the PMSM. Injecting this HF signal to the PMSM, high frequency current components are generated in the electric machine, which contains the information about the rotor position, so that these high frequency

induced components must be analysed and processed in order to isolate the component that contains the information about the rotor position [12],[13].

For doing this, a combination of different filters such as low-pass filters (LPF), high-pass filters (HPF) or band-pass filters (BPF) can be implemented in order to isolate the high frequency component that contains the rotor position [5]. The solution that is adopted in this project is based on a combination of Band-stop filters (BSF), also called notch filters, with BPF, which operate exactly in an opposite way. The BSF passes all the frequencies with the exception of those that are within a specified stop band, while the BPF isolate frequencies that are between two specific frequencies rejecting the others.

2.3.1 HF signal selection

In the selection of the HF signal that will be injected to the electric machine, there are mainly two important factors that must be analysed and taken into account, which are [5],[6]:

- **Frequency of the HF signal:** The higher the frequency of the injected signal, the higher the difference in frequency respect to the fundamental excitation signal, so that the filtering will be easier. However, the maximum frequency is limited by the switching frequency of the inverter. Usually, when it is possible, the value of the frequency is set 10 times higher than the fundamental excitation signal and 10 times lower than the power converter switching frequency.

- **Amplitude of the HF signal:** The main issue related to the amplitude has to do with the induced torque ripple. Too high signal amplitude will generate torque ripples, which is undesirable, so that the lower the amplitude of the injected signal, the lower the vibration of the electric machine due to the induced torque ripples and the lower the hysteresis losses and the losses due to the induced currents in the conductors. However, a trade off between a too high and too low amplitude of the signal must be done, since too low voltage amplitude implies loss of sensitivity since the generated current may not be enough.

The HF signal can be injected in current or voltage, being the preferred method the voltage injection. This is due to the more complexity that implies the signal injection in current, as a current regulator is needed and the injected signal is affected by its bandwidth [6],[7]. For this project, the HF signal injection in voltage is the one that will be used.

As for the kind of HF signal that can be injected to the electric machine, it can be injected in a continuous or discontinuous (transient) way, being the continuous HF signal injection the selected method in this project.

Inside this kind of HF signal injection, different signals can be also injected, being the most typical ones the **rotating sinusoidal vector injection** and the **pulsating injection**.

2.3.1.1 Rotating vector injection

By using this method, which has been proposed by Jansen and Lorenz [6],[14], a rotating voltage vector is superimposed to the fundamental excitation of the machine. This generates a high frequency induced current in the electric machine that contains the information about the rotor position, so that this generated component must be identified and isolated in order to obtain rotor position.

In this situation, the high frequency signal is injected in the stator of the machine, and as the rotor is rotating inside it, at the end, the high frequency signal is injected in the whole rotor.

Equation 2.9 shows the rotating voltage vector that is applied [6],[7].

$$V^s_{dqs_{hf}} = V_{hf} \begin{bmatrix} cos(w_{hf}t) \\ sin(w_{hf}t) \end{bmatrix} = V_{hf} * e^{jw_{hf}t} \tag{2.9}$$

Looking at equation 2.9, V_{hf} represents the amplitude of the injected rotating vector, while w_{hf} represents the frequency at which is injected.

Considering that a high frequency injection is being applied, the simplification shown in equation 2.10 can be done, so that the stator flux induced by the high frequency signal injection can be obtained by integrating the injected voltage [6],[7].

$$V = R * i + p\lambda \Rightarrow HF \Rightarrow V = p\lambda \Rightarrow \lambda = \int V \Rightarrow \boxed{\lambda^s_{dqs_{hf}} \simeq \int V^s_{dqs_{hf}}} \tag{2.10}$$

Then, substituting equation 2.9 into equation 2.10, the induced flux due to the injection of the high frequency voltage signal is shown in equation 2.11.

$$\lambda^s_{dqs_{hf}} = \frac{V_{hf}}{jw_{hf}} \begin{bmatrix} cos(w_{hf}t) \\ sin(w_{hf}t) \end{bmatrix} = \frac{-jV_{hf}}{w_{hf}} \begin{bmatrix} cos(w_{hf}t) \\ sin(w_{hf}t) \end{bmatrix} \tag{2.11}$$

The induced current due to the HF voltage signal injection can be obtained through equation 2.12.

$$\lambda = L * i \Rightarrow i = L^{-1} * \lambda \Rightarrow \boxed{i^s_{dqs_{hf}} = L_s^{-1} * \lambda^s_{dqs_{hf}}} \tag{2.12}$$

Where L^{-1} represents the inverse of the inductance matrix that can be obtained from equation 2.5 and that is shown in equation 2.13.

$$L_s^{-1} = \frac{1}{L_{ds}L_{qs}} \begin{bmatrix} \Sigma L_s - \Delta L_s cos(2\theta_r) & \Delta L_s sin(2\theta_r) \\ \Delta L_s sin(2\theta_r) & \Sigma L_s + \Delta L_s cos(2\theta_r) \end{bmatrix} \tag{2.13}$$

Substituting equation 2.11 and equation 2.13 into equation 2.12, the induced current due to the HF rotating voltage vector injection is obtained in scalar form (equation 2.14).

$$i^s_{dqs_{hf}} = \frac{-jV_{hf}}{L_{ds}L_{qs}w_{hf}} \begin{bmatrix} \Sigma L_s cos(w_{hf}t) - \Delta L_s cos(w_{hf}t + 2\theta_r) \\ \Sigma L_s sin(w_{hf}t) + \Delta L_s sin(w_{hf}t + 2\theta_r) \end{bmatrix} \tag{2.14}$$

Then, from equation 2.14, by making the mathematical developments that are shown in equations 2.15 and 2.16, the induced current can be also obtained in vectorial form as it is shown in equation 2.17.

$$\frac{-jV_{hf}}{L_{ds}L_{qs}w_{hf}}\begin{bmatrix}\Sigma L_s cos(w_{hf}t)\\ \Sigma L_s sin(w_{hf}t)\end{bmatrix} \Rightarrow \frac{-jV_{hf}\Sigma L_s}{L_{ds}L_{qs}w_{hf}} * e^{jw_{hf}t} \Rightarrow$$
$$\Rightarrow \frac{V_{hf}\Sigma L_s}{L_{ds}L_{qs}w_{hf}} * e^{jw_{hf}t} * e^{-j\frac{\pi}{2}} \Rightarrow \frac{V_{hf}\Sigma L_s}{L_{ds}L_{qs}w_{hf}} * e^{j(w_{hf}t-\frac{\pi}{2})} \tag{2.15}$$

$$\frac{-jV_{hf}}{L_{ds}L_{qs}w_{hf}}\begin{bmatrix}-\Delta L_s cos(w_{hf}t+2\theta_r)\\ \Delta L_s sin(w_{hf}t+2\theta_r)\end{bmatrix} \Rightarrow \frac{-jV_{hf}\Delta L_s}{L_{ds}L_{qs}w_{hf}} * e^{j(-w_{hf}t+2\theta_r)} \Rightarrow$$
$$\Rightarrow \frac{V_{hf}\Delta L_s}{L_{ds}L_{qs}w_{hf}} * e^{j(-w_{hf}t+2\theta_r)} * e^{-j\frac{\pi}{2}} \Rightarrow \frac{V_{hf}\Delta L_s}{L_{ds}L_{qs}w_{hf}} * e^{j(-w_{hf}t+2\theta_r-\frac{\pi}{2})} \tag{2.16}$$

$$i^s_{dqs_{hf}} = I_{pc} * e^{j(w_{hf}t-\frac{\pi}{2})} + I_{nc} * e^{j(-w_{hf}t+2\theta_r-\frac{\pi}{2})} \tag{2.17}$$

Where

$I_{pc} = \frac{V_{hf}\Sigma L_s}{L_{ds}L_{qs}w_{hf}} = \frac{V_{hf}\Sigma L_s}{w_{hf}(\Sigma L_s^2 - \Delta L_s^2)}$

$I_{nc} = \frac{V_{hf}\Delta L_s}{L_{ds}L_{qs}w_{hf}} = \frac{V_{hf}\Delta L_s}{w_{hf}(\Sigma L_s^2 - \Delta L_s^2)}$

Looking at equation 2.17, it is seen that the negative component of the induced current due to the HF signal injection is the one that contains the PMSM rotor position ($2\theta_r$), so that this component will be isolated in order to extract this information.

2.3.1.2 Pulsating injection

In this method, proposed by Corely and Lorenz [6],[15], the high frequency signal injection is done in only one axis, it wants to be injected in a concrete place of the rotor, not as in the rotating vector injection method where the high frequency signal injection is done in the whole rotor. Due to this, in this method, the high frequency signal is directly injected in the rotor.

Equation 2.18 shows this high frequency pulsating injection in the d axis [6].

$$V^r_{dqs_{hf}} = V_{hf}\begin{bmatrix}cos(w_{hf}t)\\ 0\end{bmatrix} \tag{2.18}$$

From this point, the mathematical development [6] is similar to the one that is

carried out in the rotating vector injection method, explained in **section 2.3.1.1**.

At the end, the induced current that is obtained in vectorial form is shown in equation 2.19.

$$i^r_{dqs_{hf}} = (I_{\Sigma L} + I_{\Delta L} e^{j(2\Delta\theta)}) sin(w_{hf} t) \tag{2.19}$$

Where

$I_{\Sigma L} = \frac{V_{hf}\Sigma L}{2w_{hf}(\Sigma L^2 + \Delta L^2)}$

$I_{\Delta L} = \frac{V_{hf}\Delta L}{2w_{hf}(\Sigma L^2 + \Delta L^2)}$

By using this method, the resultant currents contain a positive and a negative components that are exactly equal, which in turn can be divided into two different components as it is shown in equation 2.19, one of them that contains the rotor position information and the other that does not contain it [6].

2.3.2 HF control loop

The HF method that will be implemented in this project is based on the rotating vector injection method. A high frequency signal is injected at a certain frequency (w_{hf}) with a determined amplitude (V_{hf}) (equation 2.9), so that the final objective consist of the isolation of the induced current component that contains the rotor position of the electric machine (equation 2.17), which corresponds to negative component, in such a way that it allows to obtain the speed and position of the PMSM. Fig.2-4 shows the HF control loop that will be used in order to obtain the rotor position of the machine.

Looking at Fig.2-4, the frequency spectrum is represented and four different frequency components are shown:

- w_{2wf}: Induced current negative component frequency ($-w_{HF} + 2w_f$) that contains the rotor position (equation 2.17).
- w'_{2wf}: Induced current positive component frequency ($2w_f$) that contains the rotor position.

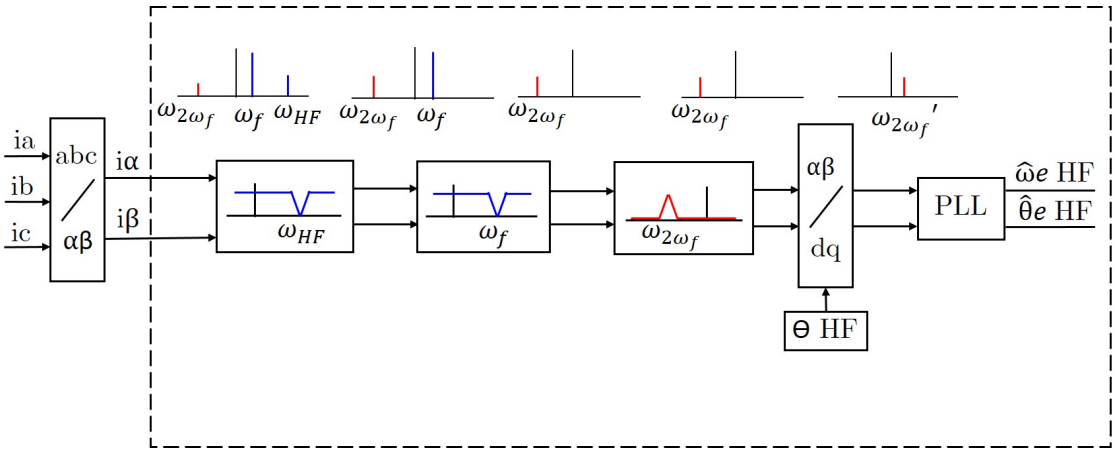

Figure 2-4: HF control loop.

- w_f: Current component at the fundamental frequency of the machine.
- w_{HF}: Current component at the frequency of the HF signal that is injected.

As for this HF method implementation, at first, the phase currents of the PMSM are transformed into $\alpha\beta$ components, and then, a combination between different kind of filters and a PLL are used in order to extract the rotor position of the electric machine.

The first filter that is used is a BSF that allows to eliminate the current frequency component at the high frequency that is being injected (w_{HF}). After that, another BSF filter is used, but in this case the frequency component that is eliminated is the fundamental component of the machine (w_f), so that at the end, only one significant component is present in the spectrum that corresponds to the induced current negative component that is required (w_{2wf}), which has a frequency of $-w_{HF} + 2w_f$. Finally, a BPF is also used to totally isolate this current component, although this filter could not be necessary depending on the electric machine.

Then, a reference frame transformation ($\alpha\beta$ to dq) is done in order to obtain a component that is only dependent on the fundamental frequency of the machine (w'_{2wf}), and finally, a PLL is used to obtain the estimated speed and rotor position of the PMSM.

Respect to the PLL configuration, it is the same as in the BEMF method (SRF

PLL, Fig.2-2, subsection 2.2.2.1), but in this situation the input signals are currents and not flux linkage.

2.4 Conclusion

Along this chapter, the sensorless control strategy has been introduced. What means using this kind of control strategy and the inherent benefits that it implies for the system are explained. Moreover, the most extended sensorless methods that are currently used, their basic operation principles along with their corresponding control loop and the PMSM equations in which they are based on have been also presented.

In the case of the HF sensorless control method, a very detailed description about the selection of the type of high frequency signal that can be injected is done along with an analysis of its characteristics in terms of frequency and amplitude.

Chapter 3

PMSM sensorless control

3.1 Introduction

The most important point of the present master thesis has to do with the implementation of the previously explained sensorless methods for their application in SIMULINK tool of MATLAB, which is the simulation tool that is selected. Along this chapter, all the required control loops and algorithms that have to be implemented in order to emulate the sensorless control of a PMSM for its application to a hybrid EV are going to be explained in detail.

3.2 PMSM system description

3.2.1 PMSM characteristics

The PMSM that is going to be used in order to apply the sensorless control technique is Surface mounted permanent magnet synchronous machine (SM-PMSM) with outer rotor configuration, which is shown in Fig.3-1 and whose main characteristics are shown in Table 3.1.

The main advantages of using an outer rotor configuration against using inner rotor configuration are the following ones [16],[17]:

- **Torque**: Outer rotor PMSMs can deliver a very high amount of torque, which

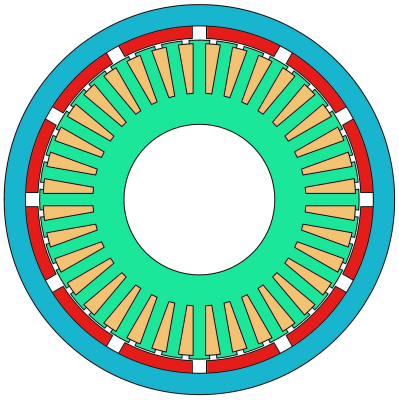

Figure 3-1: SM-PMSM with outer rotor configuration.

Parameters	**Symbol**	**Value**
Pole pairs	p	6
d axis inductance	$L_d(mH)$	0.10297
q axis inductance	$L_q(mH)$	0.12165
Stator resistance	$R(\Omega)$	0.02695
Permanent magnet flux linkage	$\lambda_{pm}(Vs)$	0.10672

Table 3.1: PMSM characteristics

makes this kind of PMSM suitable for Electric Vehicles (EV) applications.

- **Winding**: An outer rotor PMSM is easier to wind than inner rotor configurations.

- **Magnets detachment**: For an outer rotor configuration, the centrifugal force make the magnets to push against the rotor yoke, while for an inner rotor configuration, the magnets do not have a surface in opposition, so that they can detach from the rotor.

However, there is a main drawback in the outer rotor configurations, which has to do with thermal aspects. Magnets are very sensitive to the temperature, so that an adequate cooling system must be implemented. In the case of inner rotor configurations, the cooling of the magnets is easier, while in outer rotor designs, the refrigeration of the magnets is done by means of inner coolant [16].

3.2.2 PMSM control scheme

The PMSM is going to be current controlled. The machine will be rotating with a determined speed profile while different current commands are specified. Fig.3-2 shows the general control loop of the electric machine.

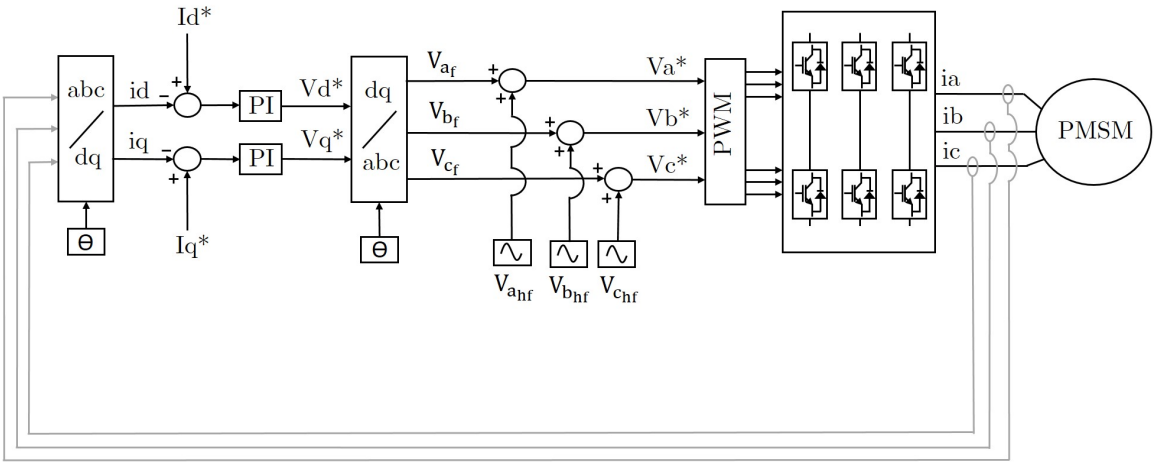

Figure 3-2: PMSM main control loop.

Where

- i_{abc}: abc currents of the PMSM
- V_{abc^*}: abc voltage commands of the PMSM
- V_{abc_f}: abc fundamental voltages of the PMSM
- V_{abc_hf}: High frequency voltage signal injection
- i_{dq^*}: Current commands in the dq reference frame
- θ: PMSM rotor position

Looking at Fig.3-2, the control scheme of the PMSM is going to be explained.

The control of the PMSM is based on the principle that the machine will be rotating at different speeds imposed by a specified speed profile while different d and q current values are commanded.

The abc currents of the PMSM are measured and transformed from the abc to the dq reference frame thanks to the rotor position of the PMSM, which is obtained from the HF and BEMF methods, and the errors between the obtained dq currents and the dq current references that are commanded are calculated. From these errors, by means of PI controllers, the required dq voltages that are needed to be applied to the PMSM are obtained in both axes and a reference frame transformation to the abc reference frame is done and the required fundamental voltages that will be applied to the PMSM are determined.

At this point, the high frequency signal injection is done. A high frequency voltage signal is added to the previous fundamental voltages, so that at the end, the abc voltage commands of the PMSM are obtained, which contain the high frequency signal that is required for the HF sensorless method. This high frequency signal injection it is disabled when the BEMF sensroless method is being used.

- **BEMF method** $\Rightarrow V_{abc_f} = V^*_{abc}$
- **HF method** $\Rightarrow V_{abc_f} \neq V^*_{abc}$

3.2.2.1 Current PIs tuning

The current control loop scheme of the electric machine with PI controllers is shown in Fig.3-3.

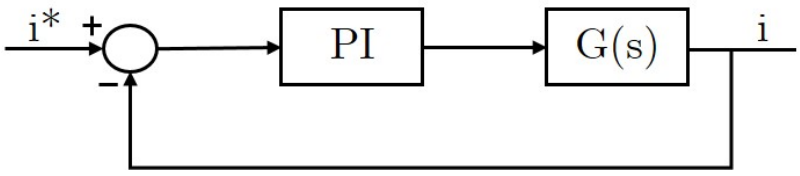

Figure 3-3: Current control loop block diagram.

For making the tuning of the current PI controllers the zero-pole cancellation method is applied. Equation 3.1 shows the typical transfer function of a PI controller.

$$PI(s) = \frac{K(s+c)}{s} \tag{3.1}$$

As the plant of the system is a motor, which consists of an RL load, the transfer function of the system is shown in equation 3.2.

$$G(s) = \frac{1}{Ls + R} = \frac{\frac{1}{L}}{s + \frac{R}{L}} \tag{3.2}$$

If both transfer functions are combined, since they are in series configuration, the equivalent block is obtained in equation 3.3.

$$G(s)' = PI(s) \cdot G(s) = \frac{K(s + c)}{s} \frac{\frac{1}{L}}{s + \frac{R}{L}} \tag{3.3}$$

Once this total transfer function is calculated, in order to eliminate the pole of the plant with the zero of the controller, the value of **c**, which is equal to the integral term of the PI controller, must be $\frac{R}{L}$. After the zero pole cancellation is done, the total transfer function $G(s)'$ is equal to $\frac{K}{Ls}$.

By solving the loop of Fig.3-3, the final transfer function is obtained as it shown in equation 3.4.

$$\frac{i}{i^*} = \frac{\frac{K}{Ls}}{1 + \frac{K}{Ls}} = \frac{\frac{K}{L}}{s + \frac{K}{L}} \tag{3.4}$$

From equation equation 3.4, the bandwidth of the system, which is equal to w, is equal to $\frac{K}{L}$, so that the proportional term of the PI controller can be obtained through equation 3.5.

$$\frac{K}{L} = w \Rightarrow K_p = wL = 2\pi fL \tag{3.5}$$

Then, in order to implement this PI controllers in MATLAB, the PI controller transfer function that is given by MATLAB in parallel configuration is shown in equation 3.6

$$PI(s) = K_p + \frac{K_i}{s} = \frac{K_p s + K_i}{s} \tag{3.6}$$

Comparing equations 3.1 and 3.6, for the MATLAB implementation, the term K_p is equal to the previously calculated term **K** (equation 3.5), and the term K_i is equal

to the term **Kc** of equation 3.1, so that at the end, if $K_i = Kc$ and c is equal to $\frac{R}{L}$ as it has been calculated before, K_i for the MATLAB implementation is equal to $K_i = K\frac{R}{L} \Rightarrow K_i = K_p\frac{R}{L}$.

Equations 3.7 and 3.8 show the proportional and integral terms for each one of the current PI controllers when zero-pole cancellation strategy is applied.

$$\begin{aligned} K_{pd} &= \boxed{2\pi f L_d} \\ K_{id} &= \boxed{K_{pd}\frac{R}{L_d}} \end{aligned} \tag{3.7}$$

$$\begin{aligned} K_{pq} &= \boxed{2\pi f L_q} \\ K_{iq} &= \boxed{K_{pq}\frac{R}{L_q}} \end{aligned} \tag{3.8}$$

Being the values of R, L_d and L_q the ones shown in Table 3.1, while the value of f has been selected to be 500 Hz.

3.3 Sensorless techniques application

In this section, a very detailed explanation about how the sensorless methods described in sections 2.2 and 2.3 are implemented for their application in the PMSM rotor position estimation is going to be done.

3.3.1 HF strategy implementation

For the HF method implementation, the input signals of the method are the phase currents of the PMSM in $\alpha\beta$ reference frame as it seen in Fig.2-5. In the general control loop of the machine (Fig.3-2), these currents are the i_{abc} currents measured from the machine, which then must be transformed to the $\alpha\beta$ reference frame.

For the implementation of this sensorless control strategy, a HF signal of 1250 Hz and an amplitude of 10 V is injected.

3.3.1.1 Filters implementation

The filtering stage of the HF sensorless method consists of three different filters in series configuration (Fig.2-4) filtering each one of them a induced current component at a determined frequency, so that at the end, the current component that contains the rotor position information can be totally isolated.

Notch filter at $\mathbf{w_{hf}}$

As it is seen in Fig.2-4, the first step that is done is to eliminate the high frequency current component that is induced due to the high frequency signal injection at 1250 Hz. For doing this, a positive sequence notch filter at this frequency is applied.

This filter only filters the component at 1250 Hz, which is the one that wants to be eliminated. The negative component at 1250 Hz will not be eliminated, since the desired component that wants to be isolated that contains the rotor position information is at a frequency of $-w_{HF} + 2w_f$ (Equation 2.17), so that if the machine is rotating at zero or at very low speeds, this filter will not eliminate this component.

Equation 3.9 shows the transfer function of this filter.

$$\frac{s - jw_{hf}}{s - jw_{hf} + w_{bw}} \tag{3.9}$$

Where w_{hf} is equal to $2\pi f$, being f equal to 1250 Hz and w_{bw} is equal to $2\pi f$, being f equal to 10 Hz, which is the selected bandwidth. The magnitude and phase of this filter are shown in Fig.3-4.

Notch filter at $\mathbf{w_f}$

The objective of this notch filter is to eliminate the current component that is at the fundamental frequency of the PMSM. As the PMSM will be rotating at different speeds, this filter must be frequency adaptive and change its frequency depending on the machine speed. The transfer function of this filter is shown in Equation 3.10.

$$\frac{s^2 + w_n^2}{s^2 + 2\xi w_n s + w_n^2} \tag{3.10}$$

Where the natural frequency of the filter (w_n) that is equal to $2\pi f$ will change the value of f depending on the machine speed and the damping factor (ξ) is equal to

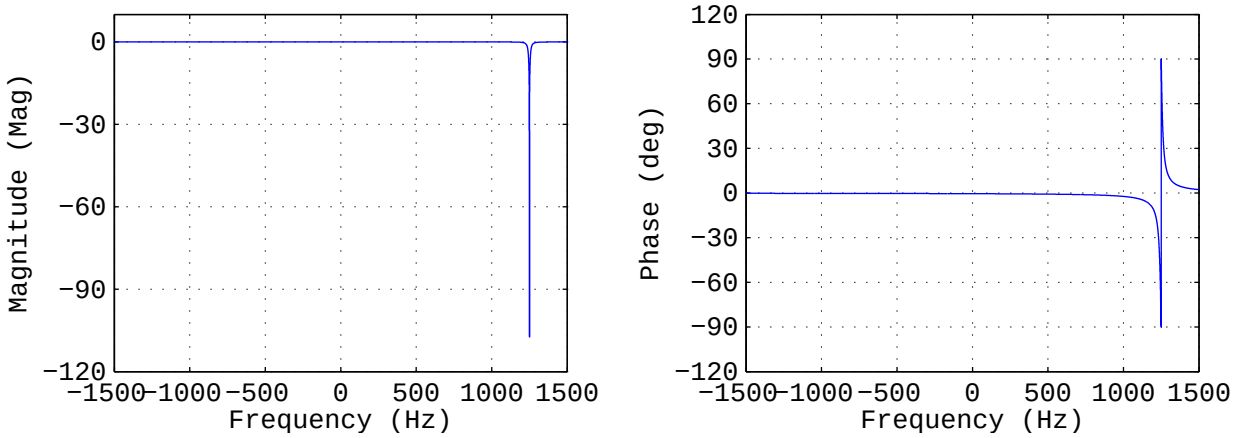

(a) Magnitude (b) Phase

Figure 3-4: Magnitude and phase of the notch filter at w_{hf}

0.2 in order to obtain a bandwidth of 10 Hz. Fig.3-5 shows the magnitude and phase of this notch filter considering a PMSM speed of 50 Hz.

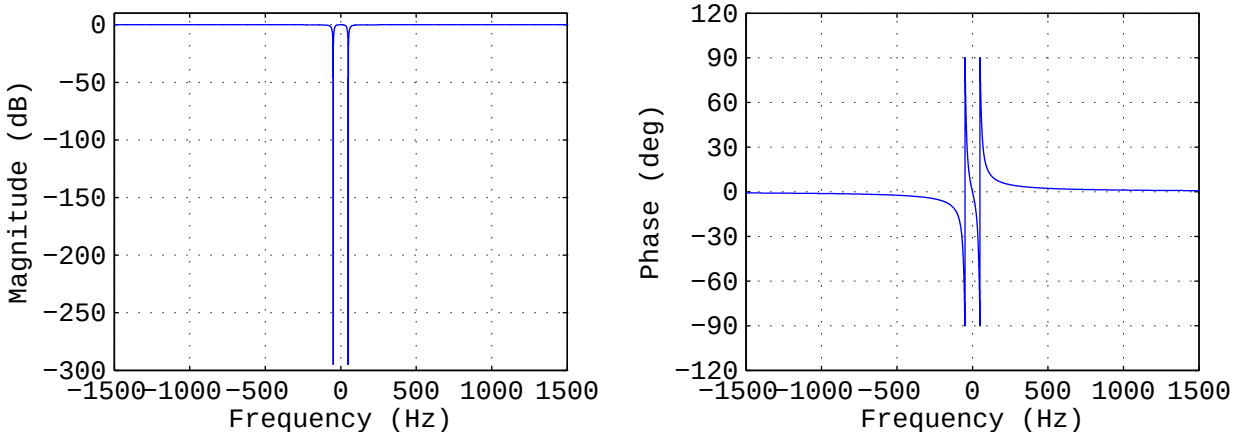

(a) Magnitude (b) Phase

Figure 3-5: Magnitude and phase of the notch filter at w_f

BPF at $(-\mathbf{w_{HF}} + \mathbf{2w_f})$

Finally, a BPF is applied to eliminate all the small current frequency components that are around the desired current component $(-w_{HF} + 2_{wf})$ and only pass this one. Equation 3.11 shows the transfer function of this filter.

$$BPF = \frac{2\xi w_n s}{s^2 + 2\xi w_n s + w_n^2} \tag{3.11}$$

Where the natural frequency of the filter w_n is $2\pi f$, being f equal to 1250 Hz at the beginning where the PMSM is stopped, and then, the filter will change its natural frequency depending on the machine speed, since this filter is also dependent on this parameter $(-w_{HF} + 2w_f)$. The value of the damping parameter ξ is 0.02 to obtain a bandwidth of 25 Hz. Fig.3-6 shows the magnitude and phase of this filter when the PMSM is not rotating (1250 Hz).

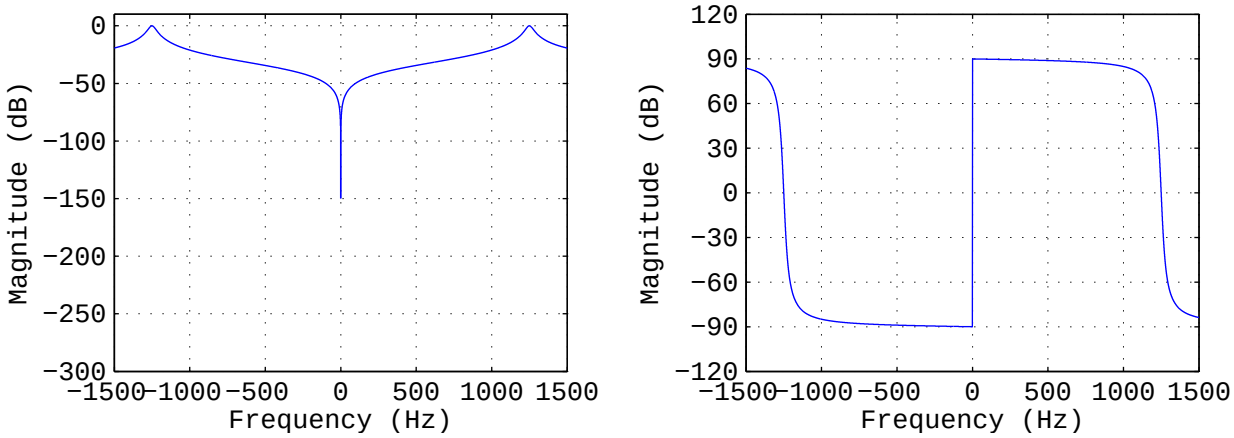

(a) Magnitude (b) Phase

Figure 3-6: Magnitude and phase of the BPF at $-w_{HF} + 2w_f$

After all these filters are applied, the desired component at a frequency of $-w_{HF} + 2w_f$ is isolated and it can be correctly analysed. Looking at Fig.2-4, a reference frame transformation to the dq reference frame with the high frequency angle (angle of the high frequency signal that is injected) is only needed to obtain the desired current component only dependent on the machine speed $(2w_f)$, and finally a PLL is used to obtain the machine speed and position estimation.

3.3.1.2 Tuning of the HF PLL PI controller

For the tuning of the PI controller of the HF PLL (Fig.2-2), the sisotool tool is used to obtain a bandwidth of around 30 Hz. For doing this, Fig.3-7 shows the system

that is introduced in sisotool.

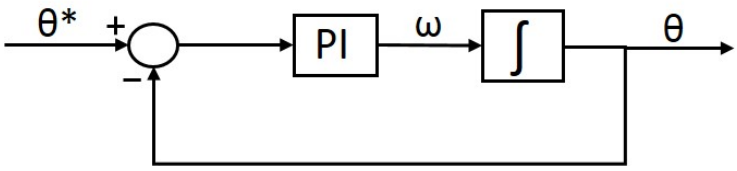

Figure 3-7: PLL block diagram for sisotool.

Looking at Fig.3-7, the plant of the system corresponds to the integrator and the gains of the PI controller are adjusted to obtain the desired bandwidth. After doing this, the calculated proportional and integral gains are the following ones:

$$kp_{HF} = \boxed{160}$$

$$ki_{HF} = \boxed{10000}$$

3.3.1.3 HF estimated position compensation

After obtaining the estimation of the PMSM rotor position, this position needs to be corrected, since the application of the different filters previously mentioned generate a phase shift of the estimated position respect to the real position of the machine. Each filter generates a determined phase shift at the frequency of the current component that wants to be isolated, which in this case is at a frequency of $-w_{HF}+2w_f$, so that at the end, there will be a combined phase shift due to the application of the different filters.

To calculate the phase shift due to each one of the filters, a fourth order polynomial that fits to the phase of the bode diagram of the corresponding filter is implemented, so that for the different frequencies at which the PMSM is rotating the polynomial of each one of the filters allows to obtain the induced phase shift at the frequency of $-w_{HF}+2w_f$. The polynomials for the different filters are created by using the "polyfit" function of MATLAB.

Then, the different filters phase shift are going to be analysed for a frequency range

between -1400 Hz to -1100 Hz, where the desired current component that contains the rotor position is located at determined PMSM speeds ($-w_{HF} + 2w_f$).

Phase shift of the NOTCH filter at $\mathbf{w_{HF}}$

Firstly, the notch filter that is applied in order to eliminated the high frequency current component (Fig.3-4) is analysed.

The discretization of the filter in order to generate the bode diagram and the fourth order polynomial that fits the phase are created for this filter. Fig.3-8 shows the results.

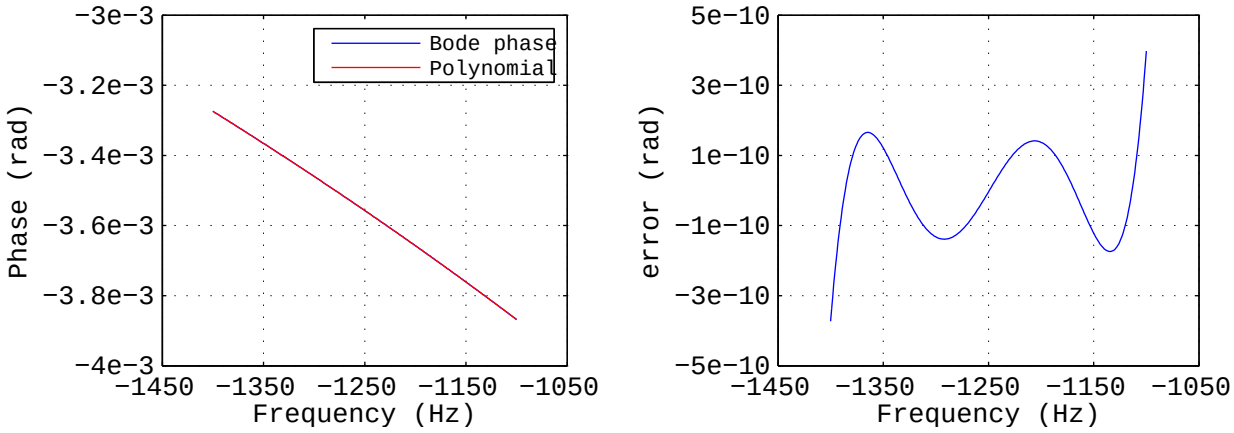

(a) Polynomial

(b) Error

Figure 3-8: 1250 Hz NOTCH filter polynomial and error at frequencies of -1400:-1100 Hz

Looking at Fig.3-8a, it shows the phase of the bode diagram and the created polynomial in the previously mentioned frequency range. As it can be seen, the created polynomial matches the phase of the bode diagram of the filter, so that the error that will be obtained by applying this polynomial, which is shown in Fig.3-8b, it is very low.

It is also seen that the induced phase shift by this filter at the frequency of the desired current component it is not so high, it is in the range of $-3*10^{-3}$ to $-4*10^{-3}$ radians.

Phase shift of the NOTCH filter at $\mathbf{w_f}$

The same procedure is carried out for the filter that is applied in order to eliminate

the current component at the PMSM fundamental component (Fig.3-5).

For this situation, Fig.3-9 shows the results.

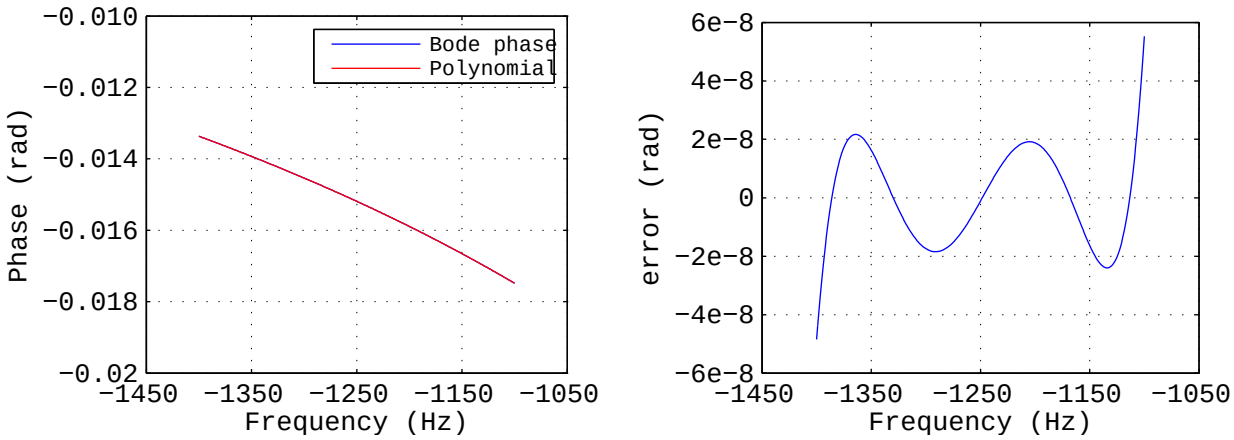

(a) Polynomial (b) Error

Figure 3-9: 50 Hz NOTCH filter polynomial and error at frequencies of -1400:-1100 Hz

Attending to Fig.3-9a, both the phase of the bode diagram of the filter and the generated polynomial are very similar and the error between them is very low (Fig.3-9b). In this situation, the induced phase of this filter at the desired current component frequency is higher than the previous one, oscillating between -0.01 to -0.02 radians.

Phase shift of the BPF at $-\mathbf{w_{HF}} + \mathbf{2w_f}$

Finally, as for the induced phase shift due to the application of the BPF used to eliminate all the small frequency components around the desired current component (Fig.3-6), it is zero, since this filter is applied exactly at the frequency of the desired current component $(-w_{hf} + 2w_f)$.

3.3.1.4 Current control loop HF components rejection

Due to the HF signal injection that is done in the HF sensorless strategy, high frequency current components enter into the current control loop of the PMSM, so that the PI controllers could react to these components making the system to fail, since an increment in the ripple of the PMSM currents occur and the HF method is affected.

In order to solve this problem, a filtering stage of two consecutive filters in series

configuration is implemented in the current control loop. One filter is fixed at a frequency of 1250 Hz, which is the responsible of filtering the high frequency current component that it is induced at the frequency that the HF signal that is being injected, and the other one is a frequency adaptive filter, which is the responsible of filtering an induced high frequency current component at a frequency of $-w_{hf} + w_f$. This last one filter starts at 1250 Hz, since the initial machine speed is 0 Hz, and then, it will change its natural frequency depending on the PMSM speed.

Fig.3-10 shows the magnitude and phase of these filters when the machine it is at 0 Hz, so that both filters are the same.

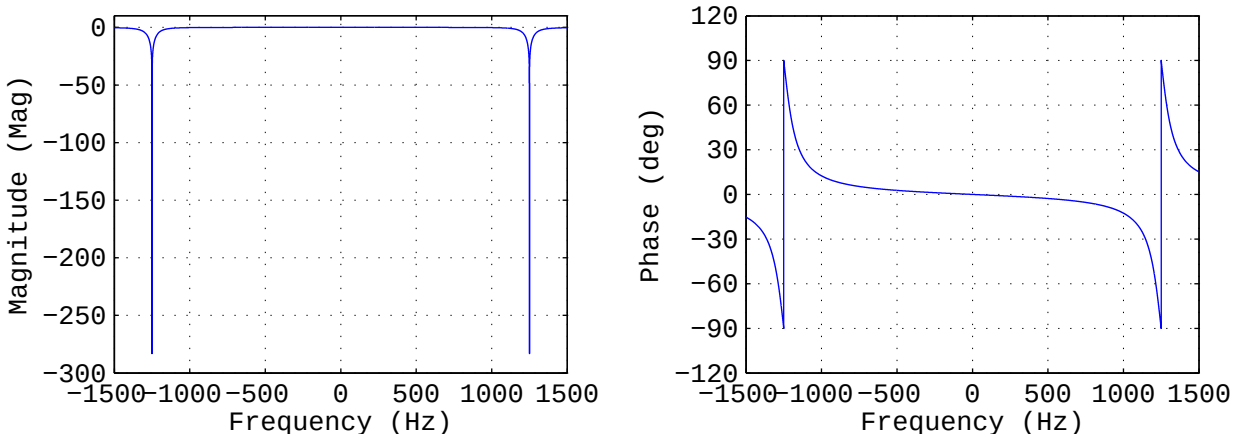

(a) Magnitude (b) Phase

Figure 3-10: Magnitude and phase of the current filters

Looking at Fig.3-10, the magnitude and phase of both filters are shown, which are the same with the difference that the frequency adaptive filter starts at 1250 Hz when the machine is not rotating and then, it starts to move in frequency as the PMSM varies its speed.

3.3.2 BEMF strategy implementation

In the BEMF sensorless strategy, the input signals are the PMSM phase currents and the terminal voltages of the machine (Fig.2-1). In Fig.3-2, these signals corresponds to the i_{abc} currents of the machine and the V_{abc} terminal voltages applied to the inverter,

which in this case are equal to V_{abc_f}, since as it has been mentioned in **section 3.1.2**, when the BEMF menthod is applied the high frequency signal injection is disabled.

3.3.2.1 Flux linkage calculation

For obtaining the flux linkage of the PMSM, which will be the input of the BEMF PLL (Fig.2-1), the integration term that is used to obtain it is implemented as a low-pass filter in the real application to avoid problems with the PLL implementation in the case of impulse signals. This is due to the fact that in case of an impulse signal occurs, the flux that will be obtained by using an integrator will remain constant at a determined value while the input signal (the impulse) returns to its initial value, so that the PLL will not correctly estimate the position of the machine. This situation does not occur by using a low-pass filter as integrator term.

The transfer function of the low-pass filter that is used is shown in equation 3.12.

$$\int \Rightarrow G(s) = \frac{1}{s + 10 * 2\pi} \tag{3.12}$$

This transfer function is implemented in order to obtain a low-pass filter bode diagram similar to the one of a integrator.

In order to see the previously mentioned difference of using an integrator or a low-pass filter, Fig.3-11 shows the output signal of both of them against a unitary impulse input signal.

As it can be seen, the output signal of the integrator remains constant at a certain value, so that in this case, the input signal of the PLL (flux linkage) will not correspond to the real one and problems in the control system can arise, while in the case of using the LPF implementation, the output value it is the same than the input.

3.3.2.2 Tuning of the BEMF PLL PI controller

The tuning of the BEMF PI controller is done by the same way of the HF PLL PI controller, it is tuned to obtain a bandwidth of around 30 Hz, so that the proportional and integral terms of the PI controller are the same as the ones of the HF PLL shown

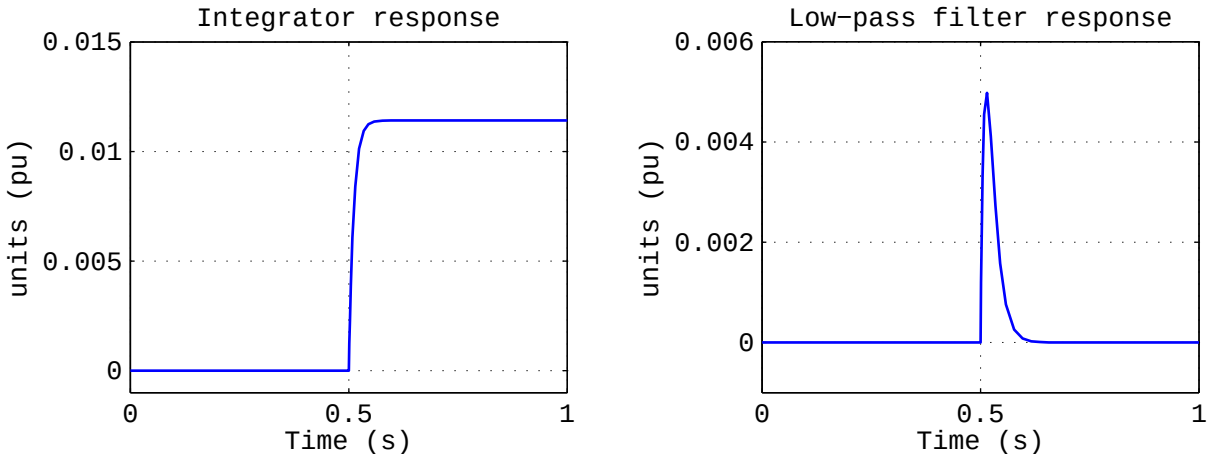

(a) integrator response

(b) low-pass filter response

Figure 3-11: Response against unitary impulse input signal

in **section3.3.1.2**:

$$kp_{BEMF} = \boxed{160}$$

$$ki_{BEMF} = \boxed{10000}$$

3.3.2.3 BEMF estimated position compensation

As in the case of the HF strategy implementation, a correction in the estimated position of the BEMF method must be done due to the induce phase shift by the low-pass filter implementation. For doing that, this induced phase shift is calculated form the LPF transfer function (equation 3.12).

At first, the implemented LPF is discretized, and then, equation 3.13 is applied [18].

$$z = e^{jwT_s} = cos(wT_s) + jsin(wT_s) \tag{3.13}$$

Once this is done, the numerator and denominator of the discretized filter are separated into the real and imaginary component as shown in equation 3.14.

$$LPF = \frac{real(num) + j \cdot imag(num)}{real(den) + j \cdot imag(den)} \tag{3.14}$$

Finally, the induced phase shifted can be obtained by subtracting the phase of the denominator from the one of the numerator of the discretized filter as shown in equation 3.15.

$$ps = tan^{-1}(\frac{imag(num)}{real(num)}) - tan^{-1}(\frac{imag(den)}{real(den)}) \tag{3.15}$$

3.4 Transition region algorithm

In the present section, a description about the transition between the two sensorless methods depending on the PMSM speed and its importance for the system properly operation is going to be explained in detail.

As it has been mentioned in sections 2.2 and 2.3, there are two different sensorless control strategies that are applied depending on the machine speed. If the machine speed is very low or zero the HF technique is more adequate, while the BEMF technique is the best option when the machine is operating at medium or high speed ranges.

Despite of the fact that the HF method is able to work at medium or high speed PMSM ranges, there are some drawbacks that makes it undesirable at these speeds, which are [19]:

- The injection of the high frequency signal at high speeds will create acoustic noise due to the pulsating torque generation, which is undesirable for the electric machine.
- Power losses generation

Due to this, a switching from one method to the other must be done depending on the machine speed.

However, a very important point must be taken into account in this situation, since a hard transition from one method to the other could make the machine control to fail. If a hard transition is done, the estimated angle that is obtained and that is used in order to make the current control of the PMSM (Fig.3-2) will change instantaneously

from the one that is obtained from the HF method to the one from the BEMF method and vice versa, so that the angle estimation in this point could change drastically and the machine control will be seriously affected making the system to fail.

In order to avoid this problem, a transition region between the two methods is established, where both of them will coexist, so that the estimated angle is changed from one method to the other in a smooth way.

3.4.1 Algorithm implementation

The implemented algorithm is based on linear functions, where the total estimated angle of the PMSM is determined as the sum of the two estimated angles multiplied by the corresponding cost of each one of the methods, so that as a function of the machine speed, each one of the methods will have a determined cost. These costs of both methods are complementary between them.

Fig.3-12 shows the costs generation as a function the machine speed.

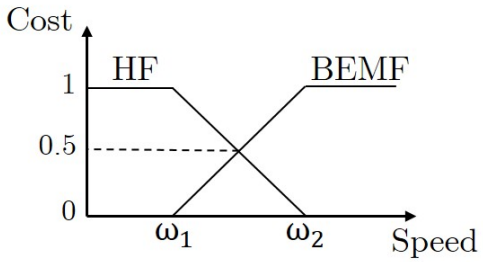

Figure 3-12: Sensorless methods costs generation.

As it is seen in Fig.3-12, there are two speeds that corresponds to the speed at which the BEMF method starts to operate (w_1) and to the speed at which the HF method is disable and the machine operates only under BEMF sensorless method (w_2).

For this project, the value of w_1 has been set to **30 electrical Hz** and the value of w_2 to **40 electrical Hz**, so that the transition region is delimited by these PMSM speeds.

The HF cost function and the BEMF cost function are implemented as follows:

$f_1(x) \Rightarrow$ **HF cost function**

- if $Speed \leq w_1 \Rightarrow HF = 1$
- if $w_1 < Speed < w_2 \Rightarrow HF = -\frac{Speed}{10} + 4$
- if $Speed \geq w_2 \Rightarrow HF = 0$

$f_2(x) \Rightarrow$ **BEMF cost function**

- if $Speed \leq w_1 \Rightarrow BEMF = 0$
- if $w_1 < Speed < w_2 \Rightarrow BEMF = \frac{Speed}{10} - 3$
- if $Speed \geq w_2 \Rightarrow BEMF = 1$

For obtaining the speed of the PMSM, which is used in order to obtain the corresponding costs in the previous function (Fig.3-12), it is calculated as the sum of the corresponding products between the calculated costs of each method by the estimated speed of the corresponding method. Fig.3-13 shows this speed calculation.

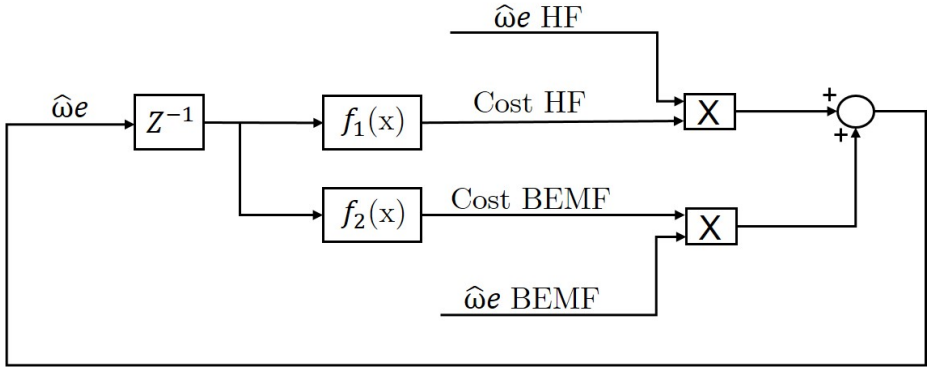

Figure 3-13: PMSM speed estimation.

Looking at Fig.3-13, $f_1(x)$ and $f_2(x)$ corresponds to the costs function of the HF and BEMF sensorless methods respectively, which are shown in Fig.3-12. For obtaining these costs, the PMSM speed estimation of the previous sample time is the one that is used, and at the end, this speed $\hat{w}_e$ is the PMSM speed estimation that is obtained by means of the HF and BEMF methods.

Then, the estimated position of the PMSM is obtained in the same way by using the costs that are obtained with the PMSM speed estimation. Fig.3-14 shows the calculation of the PMSM estimated rotor position.

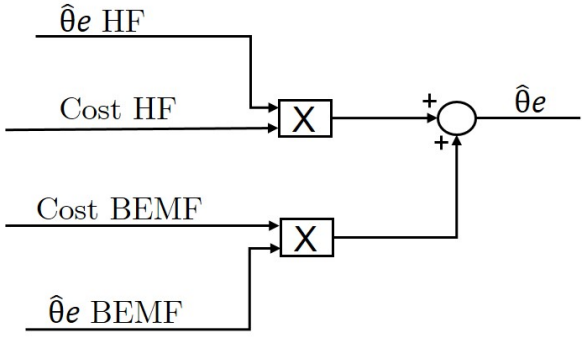

Figure 3-14: PMSM position estimation.

In this case, the costs are the same than the ones obtained in Fig.3-13, and the estimated angles that are used are the estimated angles of the corresponding sensorless methods. At the end, the estimated rotor position of the PMSM is obtained ($\hat{\theta}_e$), which is used in order to make all the reference frame transformations that are needed for the PMSM current control shown in Fig.3-2.

3.5 Conclusion

In this chapter, all the circuits, control loops and algorithms that conform the sensorless control of a PMSM have been presented and explained in detail. A description about the PMSM that is used in order to develop the sensorless control strategy along with the explanation of the desired current control loop that is applied have been done. Moreover, a very detailed explanation about the position correction that is done due to the phase shift that generates the different filters applied in both methods it is also done.

Finally, a fully detailed explanation about the implemented transition region algorithm between both sensorless methods is done, showing the algorithm that is used in order to achieve a smooth change between both sensorless methods depending on

the PMSM speed.

Chapter 4

Simulation results

4.1 Introduction

Along this chapter, some simulations in SIMULINK tool will be carried out in order to analyse the performance of the PMSM in sensorless operation taking into account all the assumptions and the implemented circuits described in **chapters 2 and 3**.

Each one of the sensorless methods are going to be analysed independently, and then, the global PMSM operation will be tested when both methods are working together. The current control loop of the PMSM and the transition region between both sensorless methods will be also analysed.

Before analysing the system, several aspects of the simulation must be remarked, which are the following ones:

- **Speed profile:** A speed profile is imposed to the PMSM in order to check the performance of the PMSM in all the different situations and to compare this speed (real speed of the PMSM) with the estimation provided by the HF and BEMF sensorless methods. Fig.4-1 shows the commanded speed profile for the simulation in electrical $\frac{rad}{s}$.

- **dq current commands:** For the d axis current the reference will be 0 Amps, while for the q axis current two current steps are set, being one of them of 50 Amps at 0.5 seconds and the second one of -100 Amps at 1.5 seconds. The

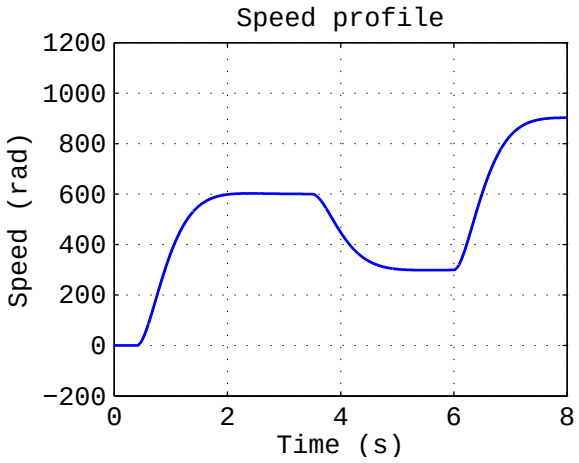

Figure 4-1: Commanded speed profile.

PMSM starts from zero speed.

- **BEMF method enable:** The BEMF sensorless method is programmed to start its operation when the machine speed is above 20 electrical Hz (200 mechanical rpm), speed at which the generated BEMF is enough for the method to give accurate measurements.

- **HF method disable:** The HF sensorless method is programmed to stop its operation when the machine speed is above 45 electrical Hz (450 mechanical rpm). At this speed the HF signal injection is disable and the machine will only operate with the BEMF sensorless method. This is implemented due to the reasons described in **section 3.3**.

4.2 Transition region algorithm analysis

First of all, the transition region algorithm is going to be analysed, since this algorithm generates the cost of each one of the sensorless methods which determine the contribution of each method to the PMSM rotor position estimation depending on the PMSM speed, including the transition between both methods at determined speeds of the machine **section 3.3**.

By applying the implemented algorithm in **section 3.3.1**, Fig.4-2 shows the cost

generation for each one of the methods depending on the speed of the PMSM, which follows the speed profile of Fig.4-1, where Fig.4-2a shows the cost along all the simulation and Fig.4-2b shows a zoom of the transition region area.

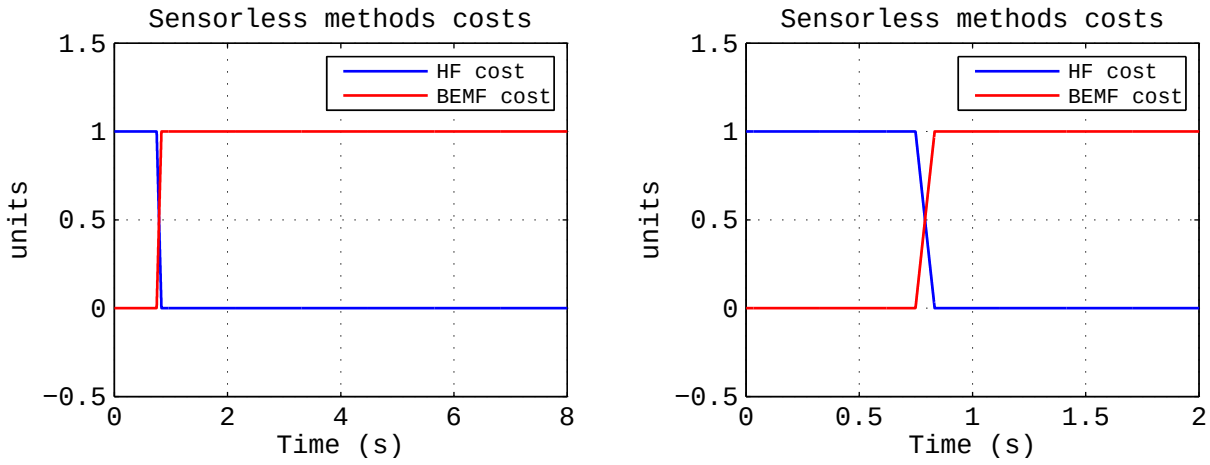

(a) Costs generation

(b) Transition region zoom

Figure 4-2: Transition region costs generation for each one of the sensorless methods

Attending to Fig.4-2a, the costs that determine the contribution of each method to the PMSM rotor position estimation are seen. At the beginning of the simulation, where the PMSM speed is not too high, only the HF method is working until the machine reaches a speed of 30 electrical Hz (188.5 electrical $\frac{rad}{s}$).

Then, from this point, a transition region between the sensorless methods starts, where their contribution to the rotor position estimation change in linear relationship according to the algorithm implemented in **section 3.3.1**, until the machine reaches 40 electrical Hz (251.3 electrical $\frac{rad}{s}$). In this transition region both methods are active. Fig.4-2b shows a zoom of this transition region.

Finally, from 40 electrical Hz, the PMSM only works under the BEMF method, being the cost of this method "1" and the cost of the HF method "0".

The PMSM rotor position estimation that can be obtained by using these costs (Fig. 3-13), which can be the position estimation of the HF method (at low speeds), the position estimation of the BEMF (at medium or high speeds) or the position estimation conformed by the contribution of both methods (transition regions), is the one that is used for the PMSM current control shown in Fig.3-1.

4.3 HF method performance

After analysing the cost generation for both sensorless methods, the PMSM performance at low speeds, where the HF method is applied, is going to be analysed.

The most important parameters that are needed to be analysed are the estimated rotor position, the error with respect the real rotor position and the estimated PMSM speed.

4.3.1 HF speed estimation

Once all the parts related to the HF sensorless method described in **chapters 2 and 3** are implemented, Fig.4-3 shows the PMSM speed estimation by the HF method and the real speed of the machine (commanded speed profile of Fig.4-1). In this graph, the speed is represented in electrical $\frac{rad}{s}$.

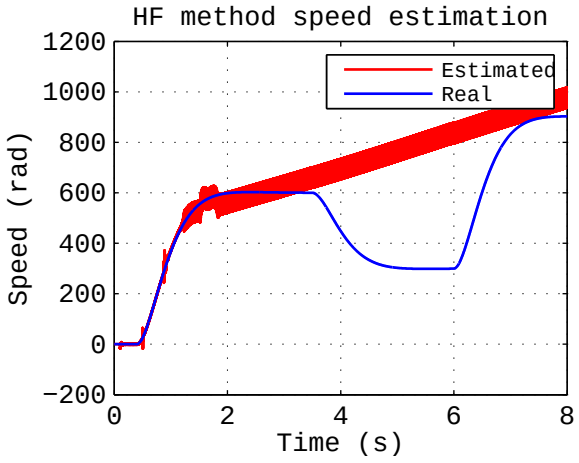

Figure 4-3: HF speed estimation.

Analysing Fig.4-3, it is seen that the estimated PMSM speed given by the HF method matches the real speed until the speed of the machine reaches 45 electrical Hz, value that corresponds to 282.75 electrical $\frac{rad}{s}$, when the high frequency signal injection is disabled (**section 4.1**).

4.3.2 HF rotor position estimation

Once the speed estimation of the machine is analysed, the rotor position estimation by using this method will be studied.

4.3.2.1 HF rotor position correction analysis

First of all, the estimated position compensation is analysed.

Fig.4-4 shows the real position of the machine, the estimated position that is obtained from the HF method and the compensated position that is obtained by using the fourth order polynomials created in **section 3.3.1.3** to compensate the induced phase shift by the filtering stage at the frequency of the desired current component.

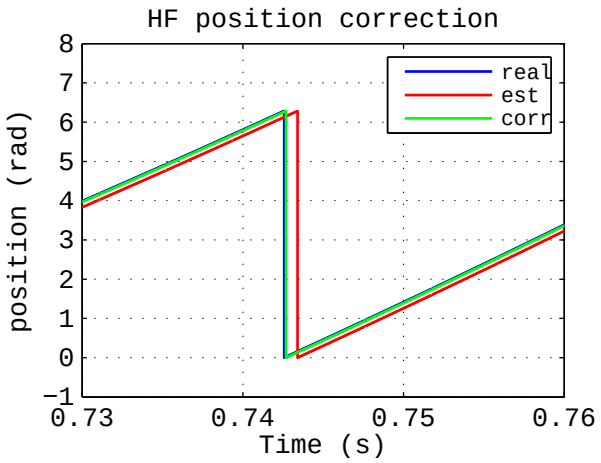

Figure 4-4: HF position correction analysis.

Looking at Fig.4-4 it is seen how the rotor position estimation that is obtained it is not so good, there is a considerable error respect to the real one due to the induced phase shift of the filtering stage. However, after the filters phase shift compensation is done, the obtained position of the machine it is quite close to the real position of the PMSM, so that the error between them it is very low.

4.3.2.2 Final HF rotor position estimation

Then, once the compensation is done, Fig.4-5 shows the estimated rotor position given by the HF method in the range between 0.65 seconds to 0.75 seconds and the error respect to the real position of the machine in the range that the PMSM is operating under this sensorless control method once the position compensation is done.

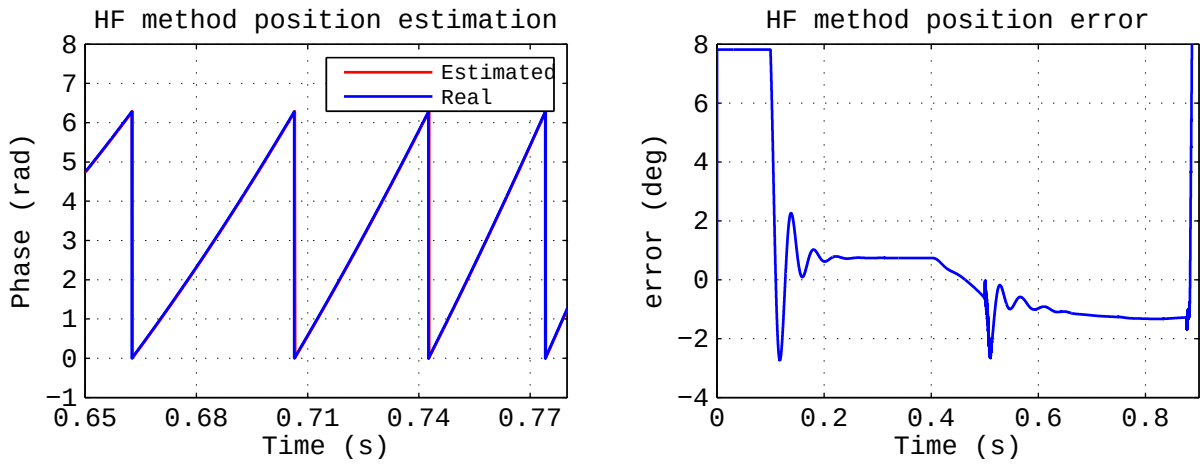

(a) Rotor position estimation

(b) Error respect real position

Figure 4-5: Rotor position estimation and error respect to the real PMSM rotor position by using the HF method

Attending to Fig.4-5a, the real rotor position and the estimated are represented in a specific time range where this HF method is working. As it is seen, the estimation of the rotor position seems to be good, but for being sure of this, a representation of the error respect to the real position in degrees in all the range that the HF method is active is shown in Fig.4-5b. Looking at this last figure, the error it is always between 2 and -2 degrees, so that the PMSM position estimation given by this sensorless method at low speeds of the PMSM it is so good. The error that appears at the beginning of the simulation is because the HF method is not enabled yet, and at the end of the graph the error becomes too high due to the HF signal injection disconnection at 45 electrical Hz.

4.4 BEMF method performance

After being analysed the HF method signals, the BEMF sensorless method is independently studied.

The BEMF method is enabled at 20 electrical Hz, as it has been mentioned at the beginning of this chapter, but its information it is not used until the machine reaches 30 electrical Hz, when the transition region between both methods starts (**section 4.2**).

For this method, as in the case of the HF method, the estimated position, the error respect to the real PMSM position and the estimated speed of the PMSM are going to be analysed.

4.4.1 BEMF speed estimation

Fig.4-6 shows the PMSM speed estimation by using this sensorless control strategy. In this graph, the speed is shown in electrical $\frac{rad}{s}$.

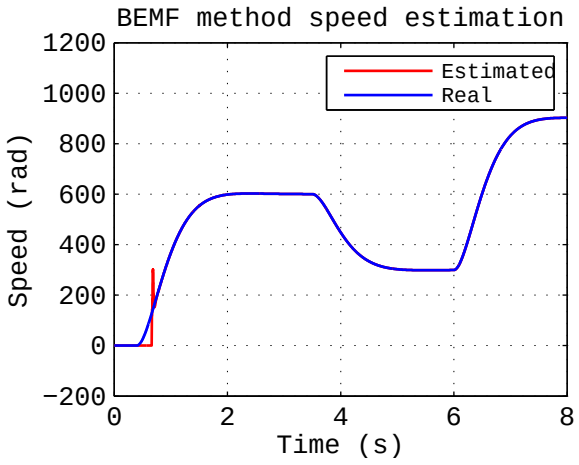

Figure 4-6: BEMF speed estimation.

Looking at Fig.4-6 it is seen that the speed estimation provided by the BEMF sensorless method is so accurate. The peak that appears in the estimated signal corresponds to the enabling of the method at 20 electrical Hz (125.66 electrical $\frac{rad}{s}$), and then, the estimated PMSM speed follows the imposed speed profile perfectly.

4.4.2 BEMF rotor position estimation

4.4.2.1 BEMF rotor position correction analysis

By the same way of the HF rotor position correction analysis (**section 4.3.2.1**), the BEMF estimated position correction is going to be analysed. Fig.4-7 shows the real position of the machine, the estimated one and the corrected position that is obtained by applying the procedure that is explained in **section 3.3.2.3**.

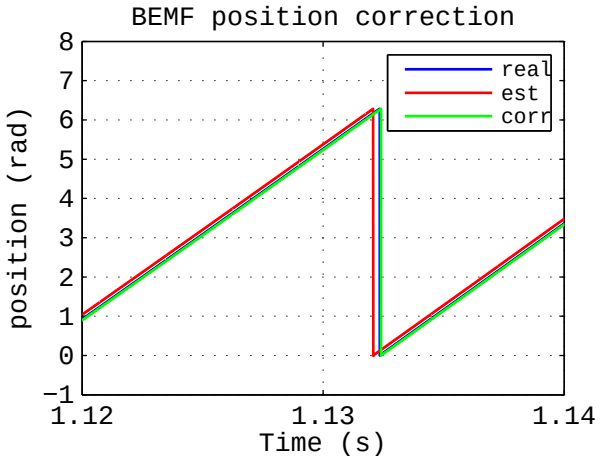

Figure 4-7: BEMF position correction analysis.

As it is seen in Fig.4-7, the corrected position that is obtained by using the phase compensation procedure, it is closer to the real position of the machine, so that the compensation it is properly done.

4.4.2.2 Final BEMF rotor position estimation

Then, final rotor position estimation of the PMSM by using this sensorless method is done. Fig.4-8 shows the estimated rotor position given by the BEMF method in a time range between 1.115 to 1.165 seconds, a period of time where the BEMF method is active, and the error respect to the real position of the PMSM when this sensorless control method is active.

Looking at Fig.4-8a, it is seen that the real rotor position of the PMSM and the estimated one are very similar between them. For checking that, Fig.4-8b shows the

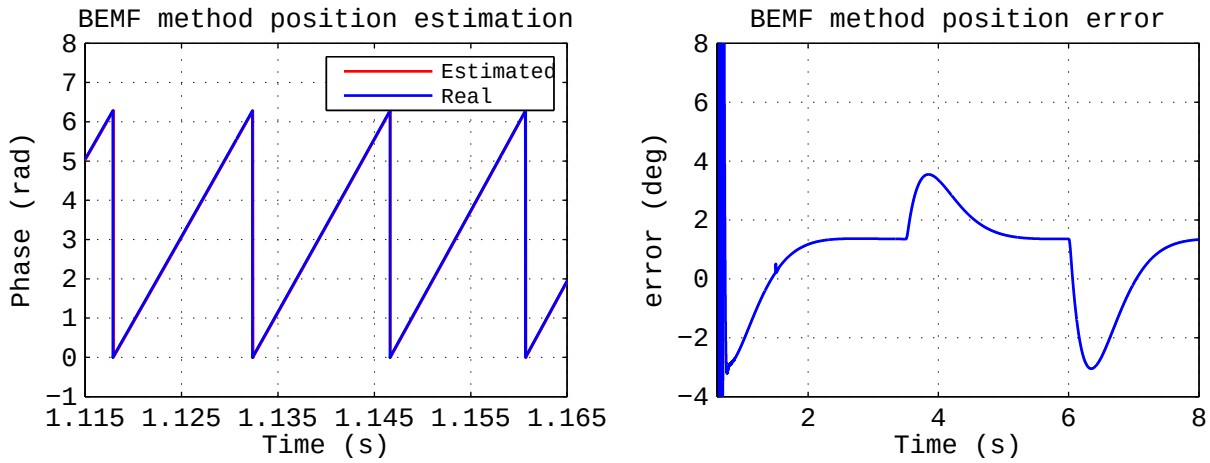

(a) Rotor position estimation

(b) Error respect real position

Figure 4-8: Rotor position estimation and error respect to the real PMSM rotor position by using the BEMF method

error respect to the real position, which is seen to be very low. The error along all the BEMF method operation, which goes from the BEMF method enable until the end of the simulation due to the speed profile characteristics, it is only between 4 and -4 degrees.

4.5 PMSM performance

After the analysis of each one of the sensorless methods that control the PMSM depending on its speed, the global performance of the system is going to be analysed. For doing this, the speed estimation of the PMSM along all the simulation, the rotor position estimation and its error respect to the real one, and the current control loop analysis of the machine under sensorless control strategy are needed to be studied.

4.5.1 PMSM speed estimation

First of all, the analysis of the PMSM speed estimation is going to be done. Fig.4-9 shows the PMSM speed estimation and the real speed of the PMSM (speed profile) in electrical $\frac{rad}{s}$, where Fig.4-9a shows the real estimated PMSM speed (without filtering it) and Fig.4-9b shows the estimated PMSM once it is filtered.

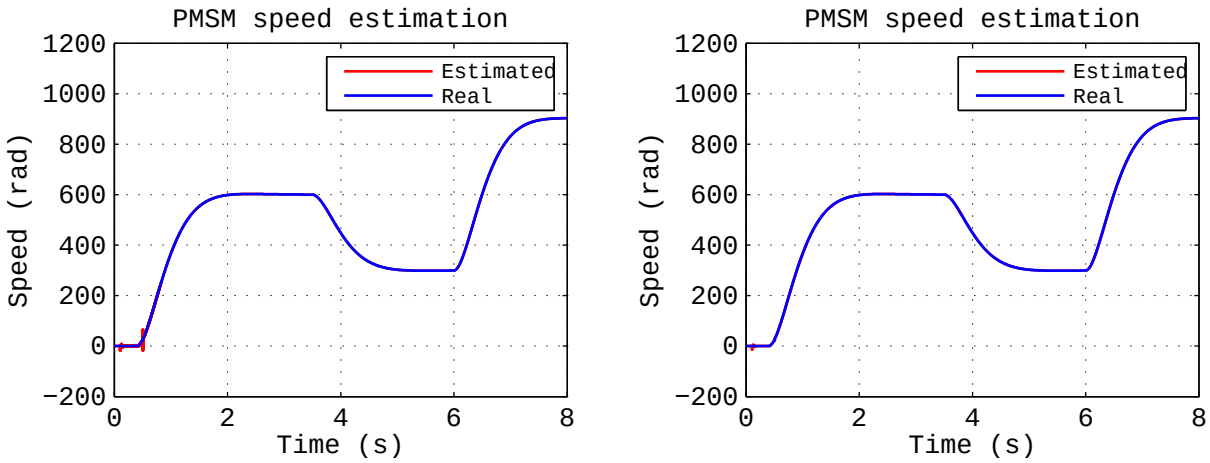

(a) PMSM speed

(b) PMSM filter speed

Figure 4-9: PMSM speed estimation

Looking at Fig.4-9a, it is seen that the estimated PMSM speed is a combination between the speed estimation provided by the HF method (Fig.4-3) and the BEMF method (Fig.4-6). The speed estimation it is so good, and only a peak at the beginning of the simulation due to the HF estimation occurs because of the q axis current change from 0 to 50 Amps at 0.5 seconds. However, by means of a low pass filter of natural frequency w_n equal to 100 Hz this peak can be filter. Fig.4-9b shows the estimated PMSM speed once this filter is applied.

4.5.2 PMSM rotor position estimation

After the speed analysis, the rotor position estimation study is going to be done. Fig.4-10 shows the estimated rotor position of the PMSM during a period of time that goes from 0.74 seconds to 0.84 seconds, which corresponds to the transition period time range (between 30 and 40 electrical Hz), and the error respect to the real position of the machine during all the PMSM operation.

Looking at Fig.4-10a, both the estimated position of the machine and the real one are shown and it is seen that they are very similar. To check that, Fig.4-10b shows the error of both signals in degrees, which is seen to be very low, with a maximum error of 4 degrees along all the simulation. Looking at this last figure, it can be

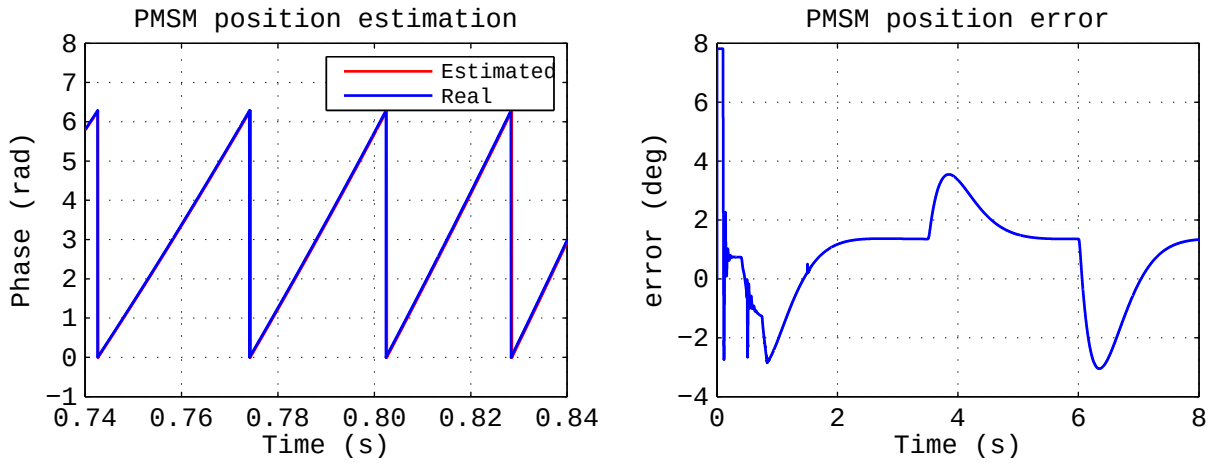

(a) Rotor position estimation

(b) Error respect real position

Figure 4-10: Rotor position estimation and error respect to the real PMSM rotor position by applying sensorless control strategy

appreciated that the error of the machine position is the composition of both errors previously analysed in **sections 4.3.2.2 and 4.4.2.2** provided by the HF and the BEMF control methods.

4.5.3 PMSM current control loop performance

Finally, as for the analysis of the PMSM operating under sensorless control, the analysis of the main control loop of the electric machine is going to be done. For doing that, the d and q axis currents of the machine will be studied in order to check how they track their respective reference commands.

Fig.4-11 shows the q axis current reference command and the q axis current of the PMSM operating under sensorless control, which suppose with the estimated rotor position provided by the HF and BEMF methods depending on the machine speed.

Looking at Fig.4-11, it is seen how the q axis current of the machine correctly follows the commanded reference. It is also seen a peak in the current when it is at 50 Amps that corresponds to the high frequency signal injection disabling, but then, it returns very fast to the desired value.

Then, the same analysis is done for the d axis current of the PMSM, which is shown in Fig.4-12.

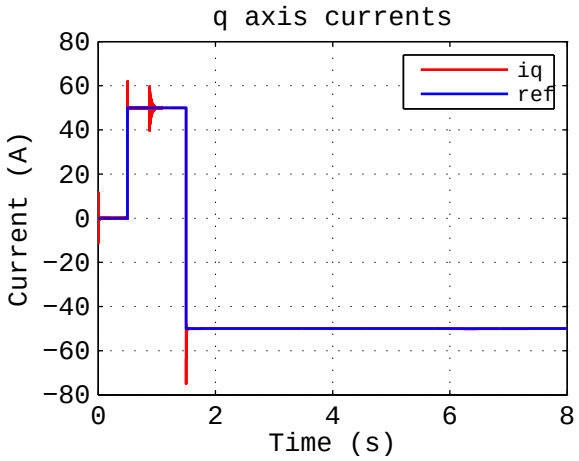

Figure 4-11: q-axis current of the PMSM under sensorless control strategy.

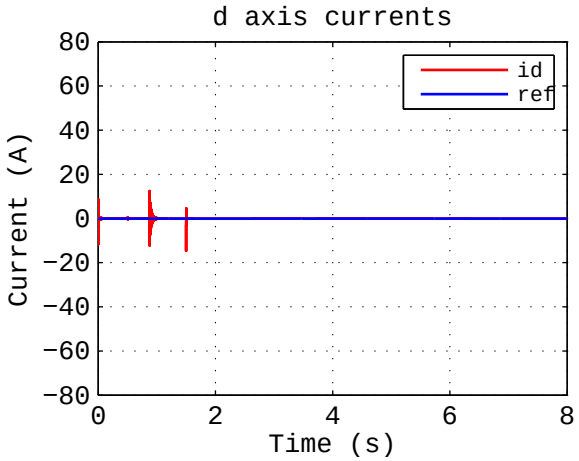

Figure 4-12: d-axis current of the PMSM under sensorless control strategy.

Attending to this figure, it is seen that the d axis current reference command is always zero Amps and the machine d axis current follows it correctly. In this analysis, there are two peaks in the current of the machine, where the first one corresponds to the high frequency signal disabling as in the case of the q axis current, and the second one to the cross-coupling due to the change in the q axis current reference (50 to -50 Amps). However, after both of them, the current returns to zero Amps very fast.

4.6 Conclusion

In this chapter, the simulation results of the complete system have been presented and the good performance of the PMSM operating under sensorless control strategy have been demonstrated. The implemented sensorless control methods and the different algorithms and circuits that are used in order to estimate the position of the PMSM, such as the implemented transition region algorithm or the implemented filtering stages that allow to correct the estimated position of the machine, show very good results in the whole speed range at which the electric machine is simulated, in terms of speed and position estimation, allowing a quite good current control of the machine without the need of using a position sensor in the rotor of the PMSM.

Chapter 5

PMSM experimental results

5.1 Introduction

In this chapter, some tests are going to be carried out with the real PMSM in order to analyse the rotor position estimation provided by the different sensorless methods that have been studied in the previous chapters in real operation. For doing that, the different control loops, filtering stages and circuits that have been explained in **chapters 2 and 3** and that are needed for each one of the sensorless control methods (BEMF and HF) are programmed in the Code Composer tool. In this part of the thesis, a previous work in this field has been used, where a sensorless control of a PMSM has already programmed and only some parameters of the system such as PI controllers or some aspects of the different control loops were needed to be changed. For carrying out the different tests, the workbench that is explained in **section 5.2** is used.

As for the different analysis that will be done along this chapter, at first, the rotor position estimation provided by each one of the sensorless control methods is going to be studied as in **sections 4.3 and 4.4**, and then, the PMSM performance when both methods combine their rotor position estimation by means of the transition algorithm will be evaluated as in **section 4.5**.

For doing these analysis, as the memory of the DSP that is used is not enough to store all the required data along a speed profile as the one shown in Fig. 4-1, what

is done is to vary the speed of the PMSM from 30 to 660 electrical $\frac{rad}{s}$ in steps of 30 $\frac{rad}{s}$ and store all the required data at the different speeds during 0.3 seconds.

5.2 Workbench

For being able to perform the different tests with the real PMSM, a workbench as the one shown in Fig.5-1 is used.

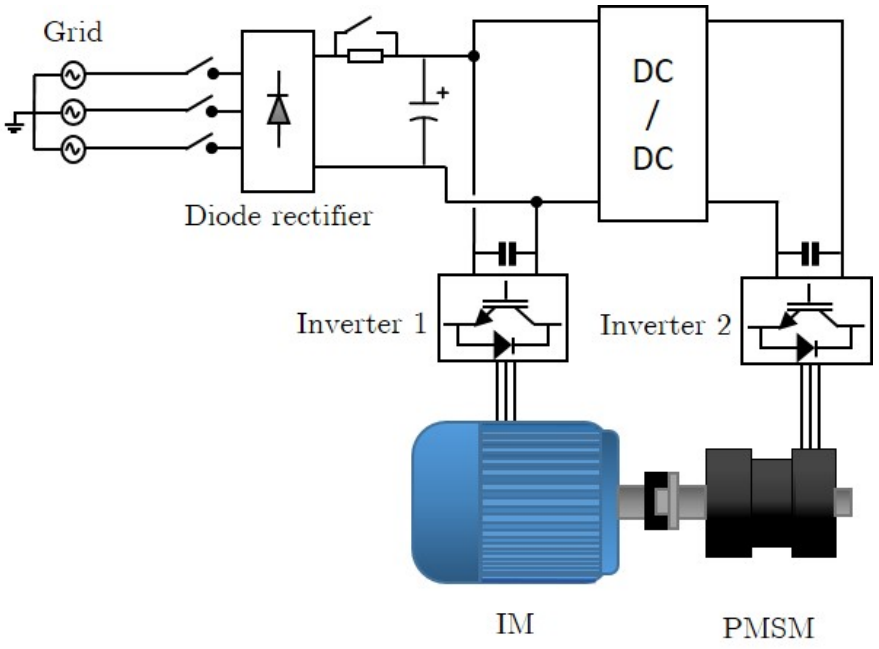

Figure 5-1: Tests workbench diagram.

Looking at Fig.5-1, the power converter configuration that is used it is very similar to a back to back converter configuration, with the difference that both electric machines do not share the DC bus, there is a DC/DC converter in the middle. With this special configuration, tests with different electric machines can be done, since the DC/DC converter allows to change the voltage at the right side of the system to adapt it to the machine requirements, in this case to the nominal voltage of the PMSM that will be used to make the experiments, which is 450 V.

5.2.1 Workbench operation

Attending to the presented system in Fig.5-1, the grid voltage is rectified by means of a diode rectifier, so that the grid phase voltage of 400 V is rectified to 565 V, which is the voltage at which the IM works. The power resistor that is placed at the output of the diode rectifier is used to charge the DC bus, and once it is charged the resistor is bypassed in order to avoid losses.

The DC/DC converter that is in the middle of the DC bus allows to have two different voltages at both sides of the converter, being 565 V at the left, which is the voltage at which the IM works, and 450 V at the right of the system, which is the nominal voltage of the PMSM.

As for the control part of the system, as it has been said before in **section 5.1**, the PMSM will be test at different speeds in order to evaluate the rotor position estimation in different situations. For doing this, the IM is speed controlled and thanks to the coupling between both electric machines the PMSM, which is current controlled (Fig.3-1), will rotate at the same speed, so that the different rotor position estimations provided by the implemented sensorless control methods at the different speeds that are set from 30 to 660 electrical $\frac{rad}{s}$ can be studied. The speed control loop of the IM is shown in Fig.5-2.

For being able to control both electric machines, two control PCBs are used, one being the responsible of analysing the electric machine data and the other one being the responsible of controlling the corresponding electric machine using the previously analysed information, in current in the case of the PMSM and in speed in the case of the IM.

5.3 HF experimental results

First of all, the HF sensorless method is analysed at a speed of 150 electrical $\frac{rad}{s}$, which corresponds to around 24 electrical Hz, approximately the speed at which the PMSM is rotating in Fig. 4-4a, where the HF rotor position estimation is analysed for the simulation results.

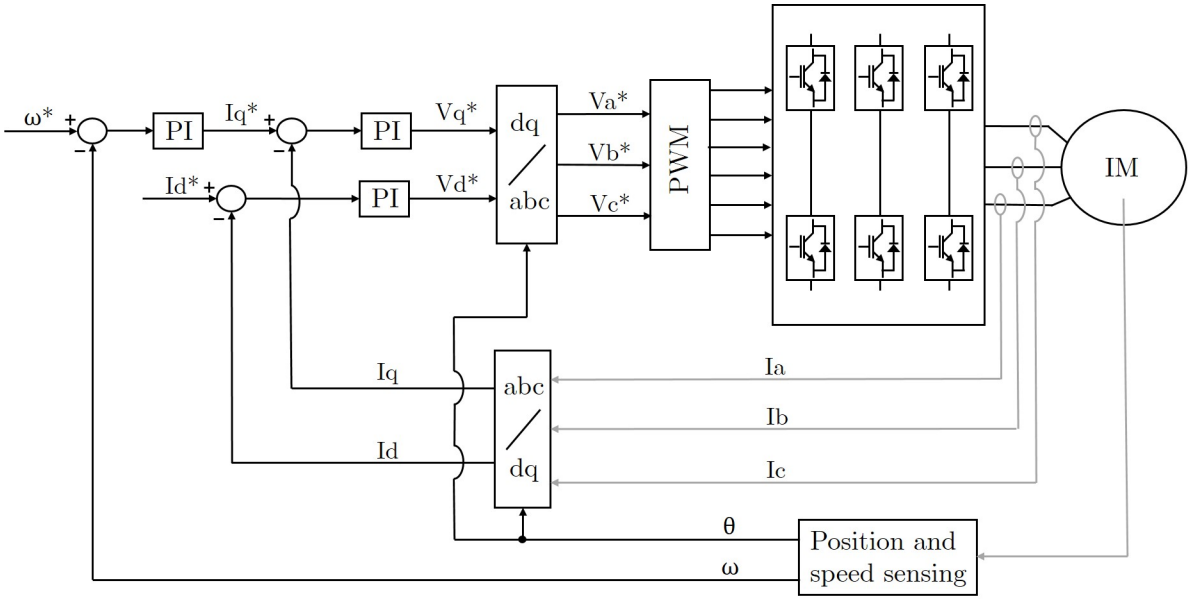

Figure 5-2: IM current control loop.

As in the case of the simulation results analysis (**section 4.3**), the estimated rotor position provided by this sensorless method and the error respect the real position are going to be analysed along with the estimated position correction that is done in order to compensate the filters phase shift.

5.3.1 HF rotor position estimation results

5.3.1.1 HF rotor position correction results

As it was shown in **section 4.3.2.1**, in order to obtain a good position estimation, the phase shift caused by the filtering stage that is done in the HF method must be compensated. Fig.5-3 shows the real position of the PMSM, the estimated one and the corrected position.

Looking at Fig.5-3, it can be seen how the estimated position error respect to the real one it is so high, but then, once the compensation is done, the error respect to the real position becomes lower resulting in the error shown in Fig.5-4b.

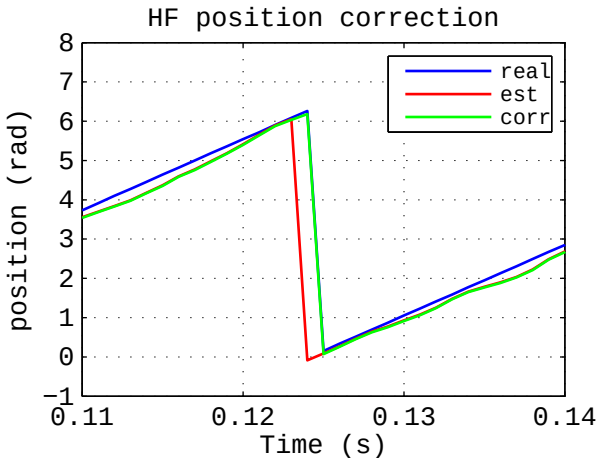

Figure 5-3: HF position correction analysis under PMSM real operation.

5.3.1.2 Final HF rotor position results

Then, once the compensation is done, Fig.5-4 shows the rotor position of the PMSM estimated by the HF method and the error respect to the real position of the machine, which is measured by an encoder.

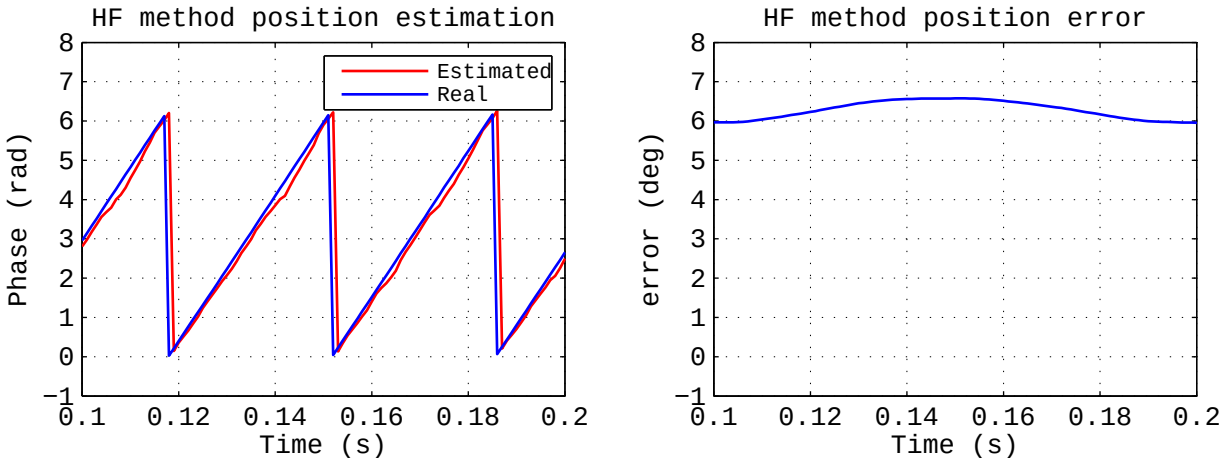

(a) Rotor position estimation

(b) Error respect real position

Figure 5-4: Rotor position estimation and error respect to the real PMSM rotor position by using the HF method under PMSM real operation

Looking at Fig.5-4a, the estimated and real position of the PMSM are seen, which are similar as it is expected. The error that exists between them is shown in Fig.5-4b, which is 6 degrees, higher than the obtained by simulations (Fig.4-4b), but an ac-

ceptable error. This difference could be due to the different behaviour of the machine in a real situation compared with the simulation, so that the PI regulators of the HF PLL could operate in a slightly different way.

5.4 BEMF experimental results

The same analysis is carried out for the BEMF sensorless method. In this case, the study is done at a speed of 360 electrical $\frac{rad}{s}$, around 57 electrical Hz, which is approximately the speed at which the machine is rotating in the simulation analysis of the BEMF (Fig. 4-7).

The rotor position estimation of the BEMF method, its error respect to the real position and the position correction that is done due to the use of filters are going to be analysed.

5.4.1 BEMF rotor position estimation results

5.4.1.1 BEMF rotor position correction results

The estimated position correction that is done in this sensorless method due to the LPF that is used in order to obtain the flux of the machine is shown in Fig.5-5.

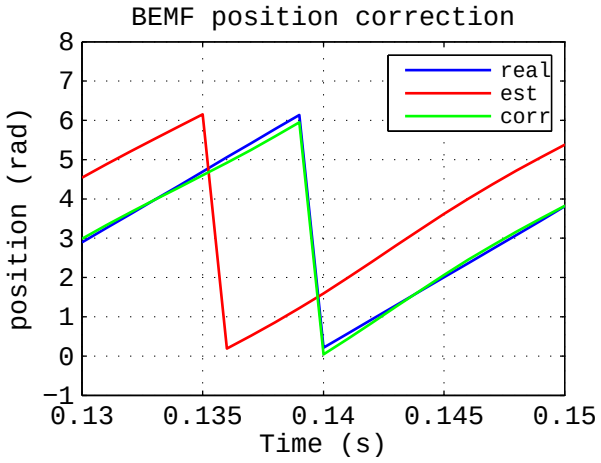

Figure 5-5: BEMF position correction analysis under PMSM real operation.

Attending to this figure it is clearly seen the important correction that is done in

the estimated rotor position. The position that is calculated by the BEMF method has a significant error respect to the real position of the machine, but once the compensation of the LPF induced phase shift is done, the obtained position is very close to the real one.

5.4.1.2 Final BEMF rotor position results

Finally, Fig.5-6 shows the estimated and real position of the PMSM and the error between them.

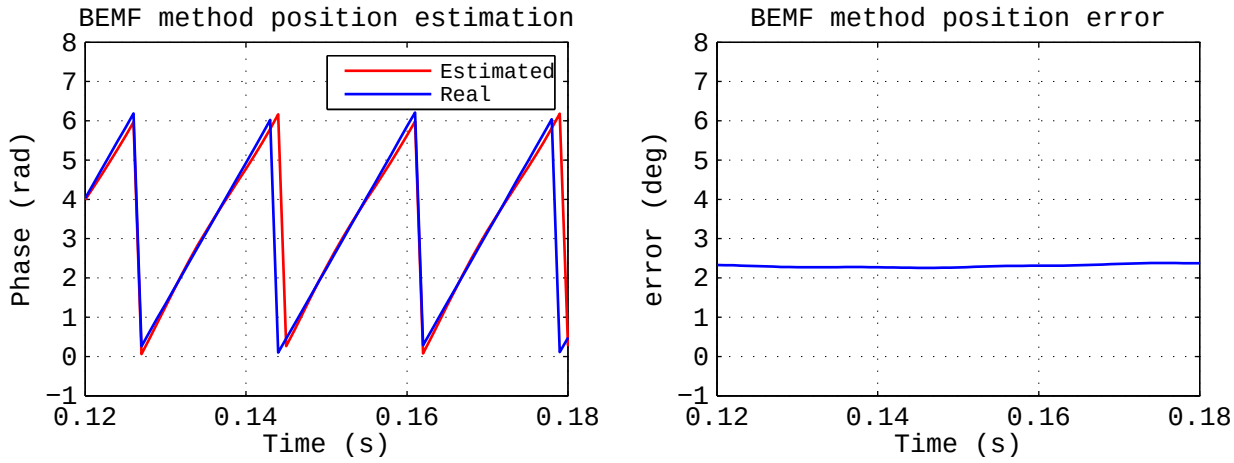

(a) Rotor position estimation

(b) Error respect real position

Figure 5-6: Rotor position estimation and error respect to the real PMSM rotor position by using the BEMF method under PMSM real operation

Looking at Fig.5-6a, it is seen that the error it is not so high between the real and the estimated position provided by the BEMF sensorlees method. For being sure of this, Fig.5-6b shows the numerical error, which is around 2 degrees, very similar to the one obtained through the simulation carried out in **chapter 4** (Fig. 4-7b).

5.5 PMSM experimental results

Once both sensorless control methods have been independently analysed, the system global operation is going to be studied. In this situation, the position of the PMSM inside the transition the region, where both sensorless methods are active, along with

its error respect to the real position of the machine will be analysed. The speed at which the analysis is carried out is 210 electrical $\frac{rad}{s}$, around 35 electrical Hz.

5.5.1 PMSM rotor position estimation results

Fig.5-7 shows the real position of the machine, the estimated position and the error between them.

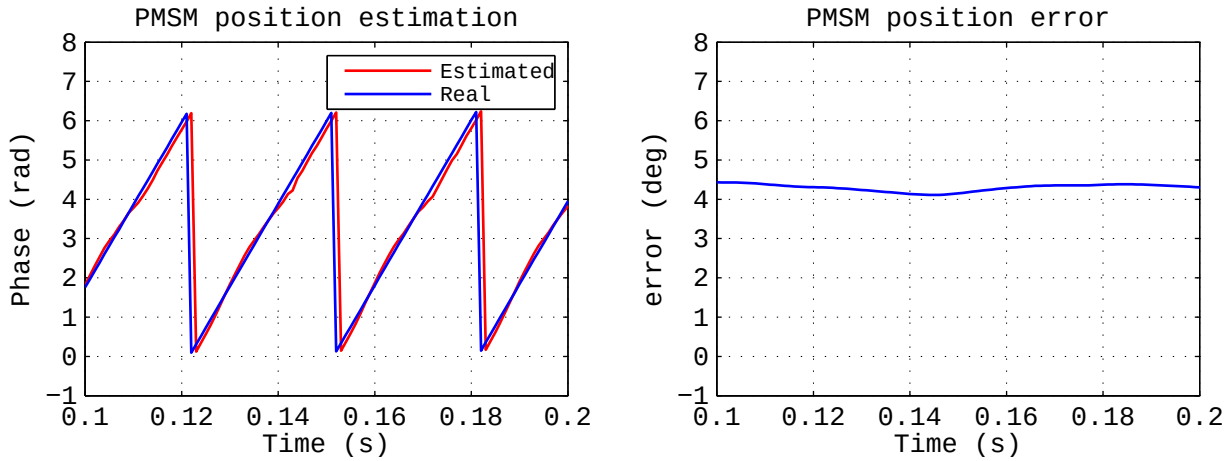

(a) Rotor position estimation

(b) Error respect real position

Figure 5-7: Rotor position estimation and error respect to the real PMSM rotor position under PMSM real operation

Looking at Fig.5-7a, it is seen that both positions are very close each other, having an error lower than 5 degrees, very similar to the one obtained through the simulation results (Fig. 4-10b).

In addition to the PMSM operation in the transition range, in this analysis of the real PMSM operating under sensorless control strategy, the error of the estimated position respect to the real one, which is obtained by means of a encoder, is analysed in all the established speed range, which goes from 30 to 660 electrical $\frac{rad}{s}$. Fig.5-8 shows this error in the whole speed range.

Attending to Fig.5-8, it is seen that at very low speeds of the PMSM, the rotor position estimation it is not so good, specifically between 0 to 60 electrical $\frac{rad}{s}$ (0 to 10 electrical Hz), which could not be solved in time. After that, the HF control method estimates the rotor position in a more accurate way (around 6 degrees of error)

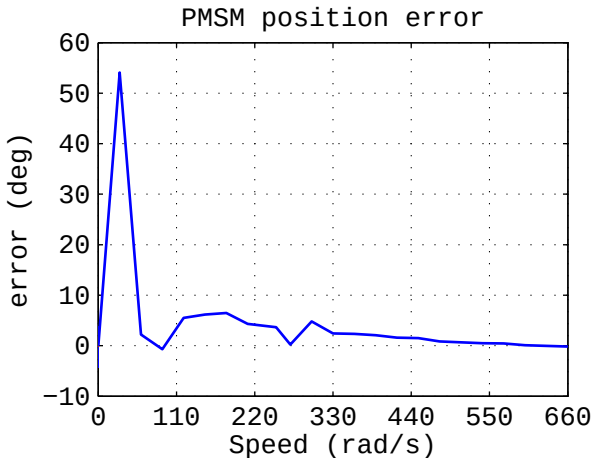

Figure 5-8: PMSM error respect to the real position from 30 to 660 electrical $\frac{rad}{s}$ under PMSM real operation.

until the transition region starts (at 180 electrical $\frac{rad}{s}$ that corresponds to around 30 electrical Hz). During this period, which lasts until 240 electrical $\frac{rad}{s}$ (around 40 electrical Hz), both sensorless control methods are working together, providing a rotor position estimation with an error between 0 to 5 degrees. Finally, from 40 electrical Hz, only the BEMF control method is working and the estimated position of the electric machine it is so accurate, with an error lower than 3 degrees.

5.6 Conclusion

In this chapter, the real PMSM operation under sensorless control strategy has been shown and studied. The previously studied and designed circuits, control loops and filtering stages in chapters 2 and 3, required for the correct operation of the HF and BEMF sensorless control methods, have been put into practice by means of the code composer tool.

The obtained results from the real operation of the machine slightly differ to the ones obtained by means of simulations in chapter 4, since in real practise the PMSM behaviour it is not the same as in simulations, but they are very close each other, so that this allows to demonstrate the correct operation of the PMSM under sensorless control strategy, obtaining accurate results in terms of rotor position estimation,

which is the most important objective of applying this kind of control strategy.

Chapter 6

Conclusions and future work

Conclusions

In the present master thesis, a very detailed study and analysis of the sensorless control strategy applied to a PMSM has been done.

The different benefits of using this kind of control strategy and the different control methods that exist in this field nowadays have been presented and described in chapter 2. The most extended ones, which are the BEMF and HF control methods, have been explained in detail understanding their basic principles and the way in which they work along with an analysis about the PMSM model equations in which they are based on.

After that, chapter 3 shows the central part of the master thesis. In this chapter the PMSM that is used for the simulations and real tests is presented and both sensorless control methods are totally implemented, showing the required filtering stages and the different circuits implementation that are necessary for each one of them. Moreover, a transition algorithm between both methods it is also implemented, which is the key of the properly operation of the machine, since it determines the sensorless methods contribution to the conformation of the rotor angle depending on the electric machine speed.

Then, the complete system is simulated in SIMULINK tool with all the implemented control loops and filtering stages, checking that PMSM works correctly under sensorless control strategy, and the results were satisfactory. Both sensorless methods

operate in the desired way depending on the machine speed, and the rotor position estimation is very close to the real one, so that the BEMF and HF sensorless control methods good performance for a PMSM sensorless control strategy it is fully demonstrated.

Finally, real tests are carried out with the real PMSM in order to check if these methods could be applied in real practise, and the same signals analysis than the ones done in the simulations are performed. The results are a bit different, since the behaviour of the real machine it is not the same as the simulated, but the rotor position estimation that is obtained for each one of the sensorless methods it is quite good.

Future work

This field it is in continuous development and a lot of improvements can be done. As it is seen along this master thesis, despite of the fact that the BEMF and HF sensorless methods provide a very good estimation of the PMSM rotor position, they are very dependent in the case of the BEMF method in the PMSM parameters accuracy and in the case of the HF method in the accuracy in which we are able to design the filtering stage and the corresponding compensation that allows to extract the rotor position. In this ambit, different algorithms that allow to avoid these dependences will be a very good option. In the same way, different sensorless methods that provide the same or better accuracy in the position estimation as these ones without the need of a high computational cost that require the use of very powerfull computers will be also a great solution.

Another possible solution that could make this kind of strategy more attractive than it is, is the development of a sensorless control method that is able to estimate the rotor position in an accurate way along the PMSM speed range, so that the transition region algorithm between different sensorless methods it is not required, which avoids a lot of possible problems, such as errors in the position estimation due to the failure of one of the methods, so that the combination of both fails, or if the speed of the machine oscillates or change too fast, possible failures in the determination of the sensorless methods contributions that could make the system to fail.

Finally, respect to the error that occur at very low PMSM speeds (**Fig. 5-8**), some improvements in the HF sensorless methods can be done in order to avoid this error, which can make the PMSM control system to fail.

Bibliography

[1] T. Finken, M. Hombitzer, and K. Hameyer, "Study and comparison of several permanent-magnet excited rotor types regarding their applicability in electric vehicles," in *Emobility - Electrical Power Train, 2010*, pp. 1–7, Nov 2010.

[2] S. Morimoto, K. Kawamoto, M. Sanada, and Y. Takeda, "Sensorless control strategy for salient-pole pmsm based on extended emf in rotating reference frame," in *Industry Applications Conference, 2001. Thirty-Sixth IAS Annual Meeting. Conference Record of the 2001 IEEE*, vol. 4, pp. 2637–2644 vol.4, Sept 2001.

[3] A. S. Z. E. D. Arafa S. Mohamed, Mohamed S. Zaky and H. A. Yasin, "Comparative study of sensorless control methods of pmsm drives," *iiste*, vol. 2, no. 5, 2011.

[4] R. A. . A. Gillström, *Sensorless Control of a Permanent Magnet Syncronous Machine using Signal Injection*. Master thesis, CHALMERS UNIVERSITY OF TECHNOLOGY, Department of Energy and Environment, Division of Electric Power Engineering, 2008.

[5] S. Medjmadj, D. Diallo, M. Mostefai, C. Delpha, and A. Arias, "Pmsm drive position estimation: Contribution to the high-frequency injection voltage selection issue," *IEEE Transactions on Energy Conversion*, vol. 30, pp. 349–358, March 2015.

[6] D. D. Reigosa, *Estudio y compensación de los efectos de la saturación y la temperatura en los métodos de control sin sensor de velocidad/posición de motores síncronos de imanes permanentes basados en el rastreo de saliencias espaciales*. PhD thesis, UNIVERSIDAD DE OVIEDO, Departamento de Ingeniería Eléctrica, Electrónica, de Computadores y Sistemas, 2007.

[7] L. A. S. Ribeiro, M. W. Degner, F. Briz, and R. D. Lorenz, "Comparison of carrier signal voltage and current injection for the estimation of flux angle or rotor position," in *Industry Applications Conference, 1998. Thirty-Third IAS Annual Meeting. The 1998 IEEE*, vol. 1, pp. 452–459 vol.1, Oct 1998.

[8] O. Wallmark and L. Harnefors, "Sensorless control of salient pmsm drives in the transition region," *IEEE Transactions on Industrial Electronics*, vol. 53, pp. 1179–1187, June 2006.

[9] Y. A. driss and D. Yousfi, "Pmsm sensorless control using back-emf based position and speed estimation method," in *Renewable and Sustainable Energy Conference (IRSEC), 2013 International*, pp. 436–440, March 2013.

[10] A. E. Driss Yousfi and A. A. Ouahman, "Efficient sensorless pmsm drive for electric vehicle traction systems," in *Electric Vehicles - Modelling and Simulations*, 2011.

[11] C. B. Charro, *Synchronization, islanding detection and power quality improvement in distributed power generation systems*. PhD thesis, UNIVERSIDAD DE OVIEDO, Department of Electrical, Computer and Systems Engineering, 2015.

[12] A. R. Setty, S. Wekhande, and K. Chatterjee, "Comparison of high frequency signal injection techniques for rotor position estimation at low speed to standstill of pmsm," in *2012 IEEE 5th India International Conference on Power Electronics (IICPE)*, pp. 1–6, Dec 2012.

[13] H. Zhu, X. Xiao, and Y. Li, "A simplified high frequency injection method for pmsm sensorless control," in *Power Electronics and Motion Control Conference, 2009. IPEMC '09. IEEE 6th International*, pp. 401–405, May 2009.

[14] P. L. Jansen and R. D. Lorenz, "Transducerless position and velocity estimation in induction and salient ac machines," *IEEE Transactions on Industry Applications*, vol. 31, pp. 240–247, Mar 1995.

[15] M. J. Corley and R. D. Lorenz, "Rotor position and velocity estimation for a salient-pole permanent magnet synchronous machine at standstill and high speeds," *IEEE Transactions on Industry Applications*, vol. 34, pp. 784–789, Jul 1998.

[16] D. Martínez, *Design of a Permanent-Magnet Synchronous Machine with NonOverlapping Concentrated Windings*. PhD thesis, Royal Institute of Technology School of Electrical Engineering Electrical Energy Conversion Stockholm 2012., KTH Electrical Engineering, 2012.

[17] D. Wu, W. Fei, P. C. K. Luk, and B. Xia, "Design considerations of outer-rotor permanent magnet synchronous machines for in-wheel electric drivetrain using particle swarm optimization," in *Power Electronics, Machines and Drives (PEMD 2014), 7th IET International Conference on*, pp. 1–6, April 2014.

[18] C. Blanco, D. Reigosa, F. Briz, and J. M. Guerrero, "Quadrature signal generator based on all-pass filter for single-phase synchronization," in *2014 IEEE Energy Conversion Congress and Exposition (ECCE)*, pp. 2655–2662, Sept 2014.

[19] M. Eskola, *Speed and Position Sensorless Control of Permanent Magnet Synchronous Motors in Matrix Converter and Voltage Source Converter Applications*. PhD thesis, Tampere University of Technology, 2006.